To the Graduate Council:

I am submitting herewith a thesis written by Jorge Antonio Ureta-Reyes entitled "Stability Analysis of Prismatic Rock Blocks." I have examined the final copy of this thesis for form and content and recommend that it be accepted in partial fulfillment of the requirements for the degree of Master of Science, with a major in Civil Engineering.

Matthew Mauldon

Dr. Matthew Mauldon,
Major Professor

We have read this thesis and recommend its acceptance:

Eric C. Drumm

Edwin G. Burdette

Accepted for the Council:

Cwminkel

Associate Vice Chancellor
and Dean of the Graduate School

STATEMENT OF PERMISSION TO USE

In presenting this thesis in partial fulfillment of the requirements for a Master's degree at The University of Tennessee, Knoxville, I agree that the Library shall make it available to borrowers under rules of the Library. Brief quotations from this thesis are allowable without special permission, provided that accurate acknowledgement of the source is made.

Permission for extensive quotation from of reproduction of this thesis may be granted by my major professor, or in his absence, by the Head of Interlibrary Services when, in the opinion of either, the proposed use of the material is for scholarly purposes. Any copying or use of the material in this thesis for financial gain shall not be allowed without my written permission.

Signature [signature]

Date July 29, 1994

STABILITY ANALYSIS OF PRISMATIC ROCK BLOCKS

A Thesis

Presented for the

Master of Science

Degree

The University of Tennessee, Knoxville

Jorge Antonio Ureta-Reyes

August 1994

DEDICATION

This thesis is dedicated with all my love to my family:

my wife Ana, and my daughters Carol and Milena,

and

my mother Leslie and grandmother Nivia

who are the most important part of my life.

ACKNOWLEDGEMENTS

..."but thanks be to God, who gives us the victory through our Lord Jesus Christ."

1 Cor. 15:57

I would like to thank my major professor, Dr. Matthew Mauldon, for his guidance and patience through the development of this research study. I would also like to thank Harry Moore, who suggested the field area for my research study. Dr. Edwin G. Burdette and Dr. Eric C. Drumm are to be thanked for serving as members on the thesis committee and providing help on clarifying important concepts of the thesis. Special thanks are for the Latino American Scholarship Program of American Universities (LASPAU - Fulbright) who gave me the economic support and the opportunity of doing this Master degree in the United States. Finally, to my friends Roberto and Barbara Benson, Ron and Theresa Ledbetter, Steve Lee, Jo and Doris Sweet, Cecil and Jane Thompson, Don and Judy Stockton, the Spanish Bible Study Group - Central Baptist Church at Bearden, the members of Grace Christian Fellowship Church in Corvallis, Oregon, and many others, my eternal gratitude for giving me the strength and support I needed to succeed during this stage of my life.

ABSTRACT

The study of problems related to the stability of wedge failure in rock cuts began approximately in the early nineteen sixties. At that time, only a few mathematical approaches in two dimensions and some graphical methods had been developed to understand the slope stability characteristics of a rock dissected by fractures and discontinuity planes, and subject to seepage and water pressures. The first studies concerning the three-dimensional stability analysis of rock slopes were made by Wittke (1965), John (1968), and Londe et al. (1969 and 1970). Years later, with the development of better computational systems, more complex analyses combining vector and graphical methods were made by Goodman (1980), Hoek and Bray (1981), Goodman and Shi (1985), Warburton (1993), and Priest (1993) among others. In the classic wedge stability problem the active resultant force $\vec{R}$ (the vector sum of weight, rock bolt forces, hydraulic forces, etc.), is resolved into components $\vec{R}_N$ and $\vec{R}_T$, respectively, perpendicular to and parallel to the potential sliding direction along the line of intersection (Z-axis). $\vec{R}_N$ is then resolved onto each of the contact planes so as to satisfy the conditions for static equilibrium. Virtually all authors assume that shear forces vanish on the XY plane. A factor of safety against sliding can then be obtained directly, either by graphical techniques (stereographic projection) or by vector analysis.

This study is based on the development of an analytical model for sliding stability analysis of prismatic blocks in rock slopes. A prismatic block is a rock block bounded by a number *n* of contact planes, where the lines of intersection of these contact planes

are all parallel. If the number of these contact planes (n) approaches infinity, the surface formed approaches a cylindrical shape, such as occurs in cylindrically-folded rocks. When the number of these contact planes is three or more, the distribution of normal forces on those planes is statically indeterminate. If the orientation of the active resultant is such that the block will attempt to move parallel to the line of intersection, the stability with respect to sliding is in addition indeterminate. To deal with these kinds of cases ($n \geq 3$), a mathematical approach is developed to determine of stability using the concept of minimum potential energy. This new model is then used to evaluate the factor of safety against sliding of prismatic blocks as a function of friction angles, block geometry, and loading conditions. The model developed is quite general and includes wedge sliding ($n = 2$) and plane sliding ($n = 1$) as special cases. To validate the model the factor of safety is calculated by the new energy-based method and the result compared with the solution for the limiting equilibrium approach, obtaining an answer that remained the same to 2 significant figures by both methods.

This analysis was used in sliding stability investigations of two road cuts with cylindrically-folded rocks located between Walland and Kinzel Springs, Blount County, Tennessee. The rock formations of these two rock cuts display conditions of instability such as rockslides, rockfalls, and dip slope failure that are barely controlled by different means such as retaining walls, steel mesh, or anchor bolts. The initial results using the new energy-based approach in these rock cuts show a significant reduction in the factor of safety of up to 14% when compared with the solution for the same type of folded rock taken as a wedge failure. Therefore, it was possible to determine that there is a reduction in the factor of safety compared with the typical wedge failure model when three or more planes of discontinuity are taken into account to form the prismatic rock block.

TABLE OF CONTENTS

TABLE OF FIGURES

CHAPTER 1

PURPOSE OF THE STUDY

1.1 Introduction

The purpose of this study is to develop a model for sliding stability of prismatic rock blocks and to apply the model to some case histories. A prismatic rock block is defined as a rock block bounded by a number *n* of contact planes, where the lines of intersection of these contact planes are all parallel[1]. Wedge and plane failures, with two and one contact planes, respectively, can be considered special cases of prismatic blocks. As the number of planes (*n*) approaches infinity ($n \rightarrow \infty$), the surface formed approaches a cylindrical shape, i.e., as in cylindrically-folded rocks. If $n \geq 3$, the stress distribution along the contact between a prismatic block and the rock mass is statically indeterminate, and therefore, the stability condition cannot be adequately described by limiting equilibrium methods such as wedge and plane models. To deal with such cases an energy-based approach is developed to evaluate the factor of safety against sliding of these prismatic rock blocks. The factor of safety is a function of friction angles, block geometry, and loading conditions.

This method is used in Chapter 4 for stability investigations of two rock cuts, which display tightly folded rocks, located between the towns of Walland and Kinzel Springs along Highway 73 in Blount County, Tennessee. In addition to the effects of

[1] In crystallographic terminology, the planes bounding a prismatic rock block constitute a *zone* which, together with their lines of mutual intersection, are parallel to a given line defined as the *zone axis* (Bloss, 1961).

folding and faulting, the rocks of the area have also been affected by a high degree of weathering that has changed the chemical composition of the original rocks. Under these circumstances the stability of slopes in the area is barely controlled by different means as retaining walls, steel mesh, or anchor bolts.

This study is divided into five chapters, the text of each of which is intended to stand by itself. The content of each chapter is describes as follows:

(a) The first chapter is a description of the purpose of the study.

(b) The second chapter presents an introduction to the concept of plane and wedge failures, and the development of the classic block theory for the past 30 years.

(c) The third chapter includes the assumptions and theoretical concepts used to develop the new mathematical approach of sliding stability regarding the concept of minimum potential energy.

(d) The fourth chapter describes the geological formation as well as the actual lithology of the study area, and summarizes the interpretation of the field data taken from the study area.

(d) Finally, the fifth chapter presents the final conclusions with respect to the sliding stability conditions of the study area.

CHAPTER 2

BASIC CONCEPTS OF STABILITY ANALYSIS OF ROCK SLOPES

2.1 Introduction

Plane and wedge failures are stability problems of rock slopes that are common both in natural slopes and in engineered cuts. Hoek and Bray (1981) summarize the main features which must exist in order that sliding can take place. Plane failures may occur when the strike of a single plane such as bedding is parallel or nearly parallel (within $\pm$ 20°) to the slope face and the weak plane dips toward the free face at an angle greater than the friction angle. Wedge failures may occur when a block defined by two planes attempts to move either parallel to one of the planes or along the line of intersection of both planar discontinuities. Both wedge and plane failures are depicted in Figure 1, taken from Goodman (1989).

For a wedge of rock bounded by failure planes, Warburton (1993) stated that the fundamental problem is to predict how the fixed surroundings and the forces acting on the block will affect its movement. Here, the important factors in the solution of stability problems are the shear strength along the geological planes, and the geometry of the slope, i.e., dip and dip direction of the discontinuity planes. If we assume that the shear stresses perpendicular to the sliding direction are zero[2], then with respect to plane and

---

2 This assumption is standard in wedge and plane sliding analysis. It is assumed that all frictional shear opposes motion.

wedge failures, the effect of friction can be determined by appropriate resolution of forces and the system of normal forces is statically determinate. It is, therefore, essential to know the friction force acting on each plane in order to assess the factor of safety against sliding for any rock block.

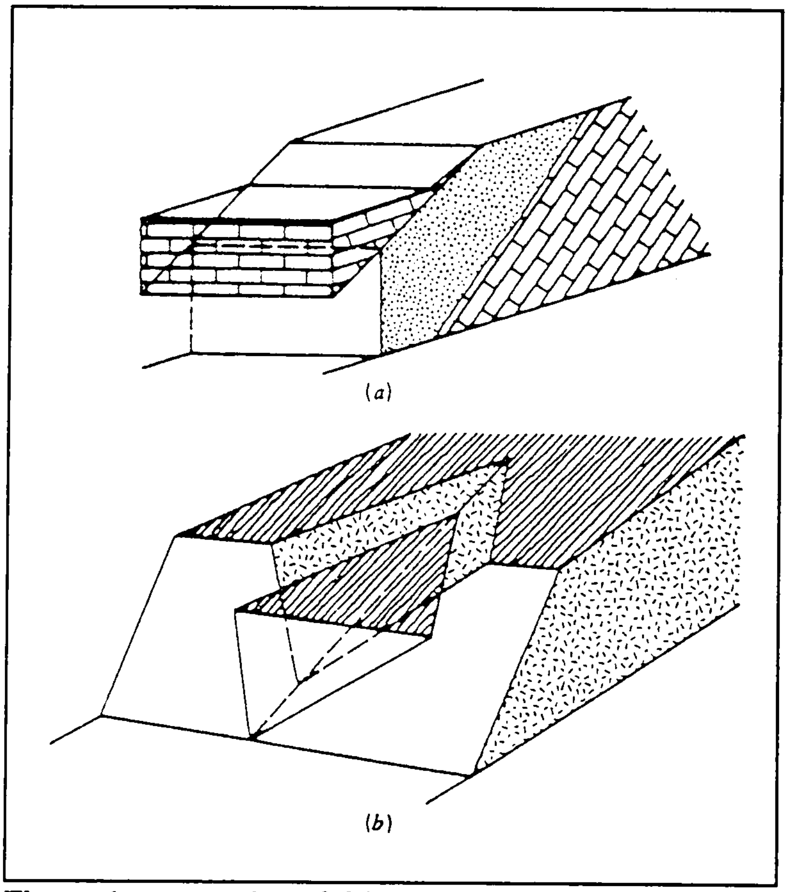

Figure 1 Modes of failure for rock slopes: a) plane failure, and b) wedge failure. (Goodman, 1989)

2.2 Previous Work

The study of problems related to the stability of wedge failure in rock cuts began approximately in the early nineteen sixties. At that time, only a few mathematical approaches in two dimensions and some graphical methods had been developed to evaluate a rock mass which is discontinuous, anisotropic, and may involve seepage and water pressure (Londe et al., 1969).

The first studies concerning the three-dimensional stability analysis of rock slopes were made by Wittke (1965), John (1968), and Londe et al. (1969 and 1970). For instance, Wittke in 1965 published the first analytical method, based on vector analysis, for determining the stability of slopes intercepted by one or two sets of joints. This analytical method considers the effect that external loads, produced by foundations, rock anchors, etc., could have on the safety of the slope against sliding. Some of the assumptions made by Wittke in his research are the following:

(a) Rock blocks can be considered to be practically rigid.

(b) There is a relatively small tensile strength across any joint plane.

(c) The forces transmitted across the joints, i.e., compressive and tangential forces, depend upon the degree of separation between the planes.

(d) The factor of safety may be reduced due to translation and rotation.

A general description of the three-dimensional vector analysis for wedge failure made by Wittke is shown in Figure 2. In this figure, the geometry of the slope, coordinate system, and orientation of the joints are defined to explain the mathematical expressions used by Wittke in the stability analysis of slopes cuts.

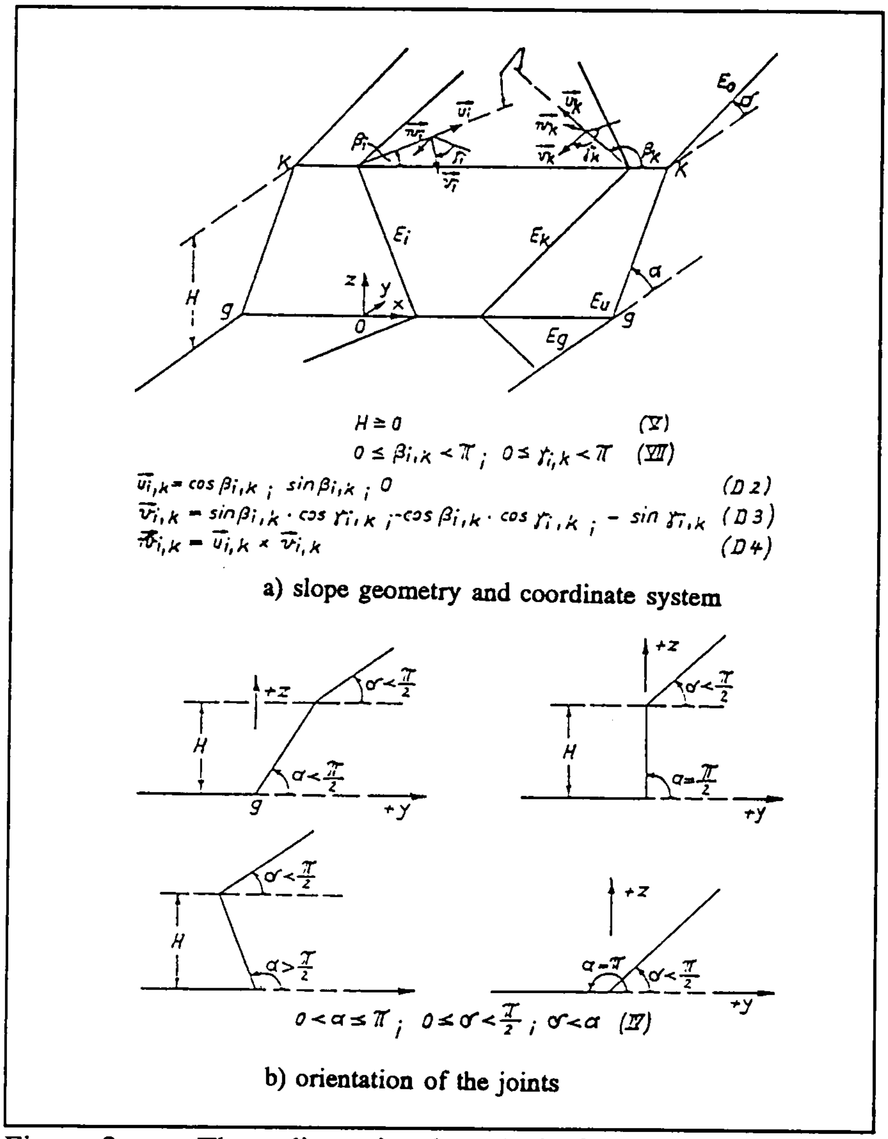

a) slope geometry and coordinate system

b) orientation of the joints

Figure 2 Three-dimensional analysis for a wedge in a rock slope (Wittke, 1965).

The contribution of John (1968) in this field was related to the development of a graphical method for stability analysis of slopes in jointed rocks. John made use of the equal-angle or Wulff stereographic nets, and the equal-area or Lambert-Schmidt nets to evaluate angular relations between geological planes. These geological planes such as joints, fissures or bedding planes were represented by lines and planes in space. The assumptions for this method developed by John can be summarized as follows:

(a) The shear resistance along the geological planes is only due to friction.

(b) Retaining forces due to rock anchors, retaining walls, or buttresses can be calculated in proportion to the weight of the rock mass to be supported.

(c) Seismic forces can be considered to act in any direction.

(d) The resultant of hydraulic thrust acting on the rock mass can be considered in the analysis if expressed in proportion to the weight of the rock mass.

(e) The rock material is competent enough that failure occurs along geological planes.

One of the applications that John used with the stereographic equatorial nets was the concept of the friction cone. This concept is used to determine the angle between a line of action of a force and a line normal to a plane. Combined with the angle of friction along this plane, this approach can be used to evaluate graphically the likelihood of sliding along this plane under a load acting in any direction. Figure 3 depicts this concept, reduced to the plane case for simplicity.

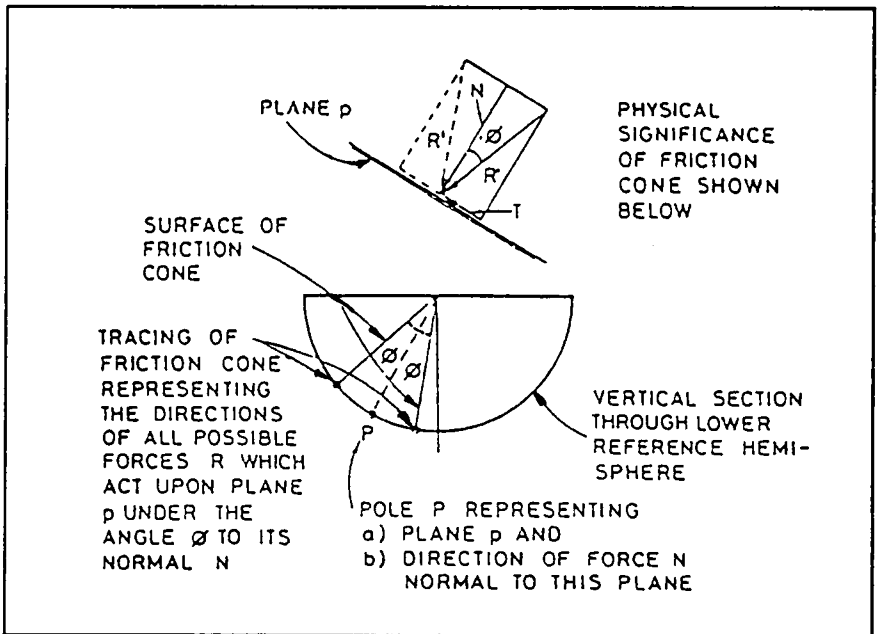

Figure 3 Concept of friction cone (John, 1968).

The same concept is expanded to three dimensions using a equatorial net with cone tracings for different angles ϕ about a pole P of a plane p, where this plane p is represented by a great circle on the equatorial net (see Figure 4). The *cone surface* illustrates the directions of all lines which have a certain angle with the normal to the plane given by the pole P. Thus, the intersection of any plane through the pole, P, with a cone surface produces the directions of the two lines which are located within this arbitrary plane and have an angle ϕ to the normal of the plane p.

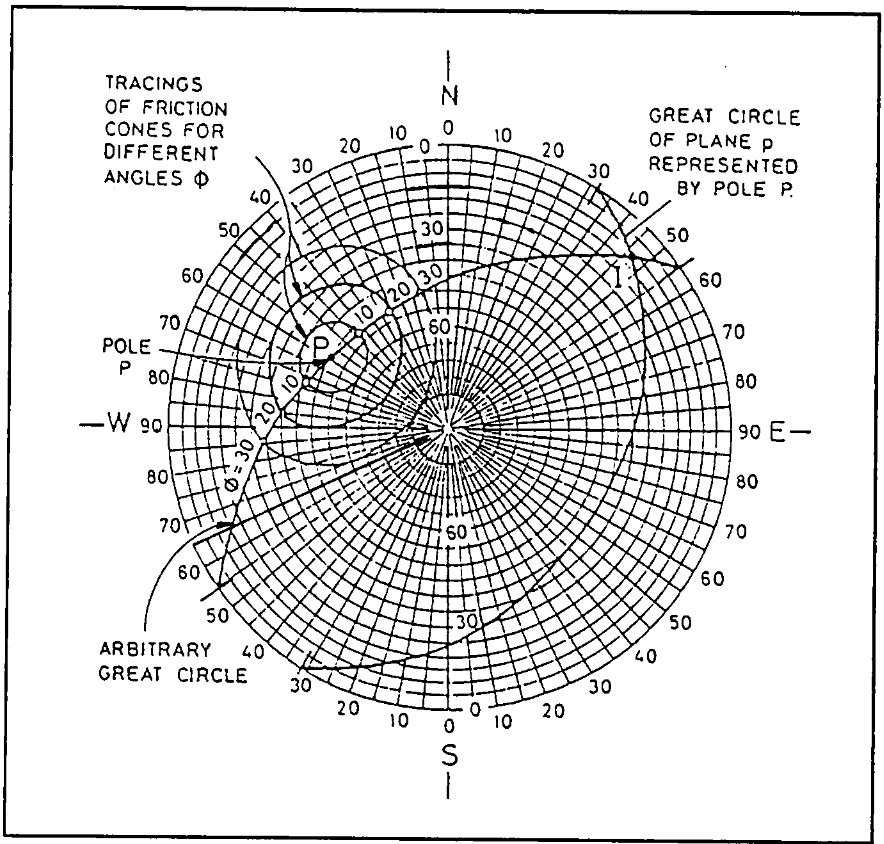

Figure 4 Equatorial net showing the application of the friction cone (John,1968).

Londe et al.(1969 and 1970) made a stability study of rock slopes using a three-dimensional approach for a fractured or faulted rock mass. This study permits one to analyze how the strength parameters, such as the total weight of the rock mass, the thrust of any type of retaining structure, the force due to earthquakes and the force due to hydrostatic uplift, are producing different forms of rupture of the contact planes and therefore affecting the stability of the rock slope. In this method, the assumptions to study the stability of a slope were made based on a given rock volume as follows:

(a) All the internal faces of the rock volume are plane, and the volume of the rock is defined by the intersection of the contact planes.

(b) The volume of the rock mass is undeformable and there is no internal rupture in the rock volume.

(c) The shear strength along the contact planes is only due to friction. Cohesion and tensile strength are regarded to have no influence on the contact planes.

(d) Only translation of the rock volume is regarded. The moments of the forces acting on the rock mass are not taken into account for equilibrium.

The statement written in point (d) was of primary importance in this research because it was assumed to facilitate the analysis of the different forms of rupture with respect to the direction of the active resultant upon a defined volume of rock mass (see Figure 5). Thus, the rupture can occur only with the separation of one, two, or three of the faces; there is sliding on two of the base planes in the first case, on one in the second case, and on none in the last case. These three possible conditions permitted to identify seven types of rupture, which were called by Londe et al. Z_1, Z_2, Z_3, Z_{13}, Z_{23}, Z_{31}, Z_{123}, as shown on Figure 5. One more type of rupture, Z_0, was added to include the case in which all the planes remain in contact and are in perfect stability.

TYPE	NATURE OF SLIDING VECTOR δ	CONTACT FACES	OPEN FACES	DIAGRAM
Z_0	–	1,2 & 3	–	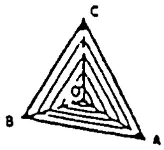
Z_1	DIRECTION OA	2 & 3	1	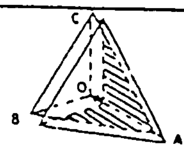
Z_2	DIRECTION OB	3 & 1	2	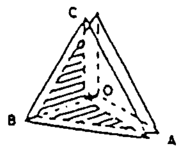
Z_3	DIRECTION OC	1 & 2	3	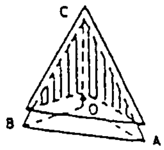
$Z_{1.2}$	ON PLANE 3 DIRECTION BETWEEN OA & OB	3	1 & 2	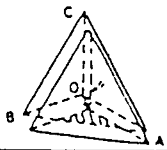
$Z_{2.3}$	ON PLANE 2 DIRECTION BETWEEN OB & OC	1	2 & 3	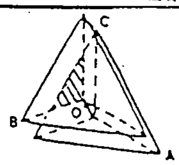
$Z_{3.1}$	ON PLANE 2 DIRECTION BETWEEN OC & OA	2	3 & 1	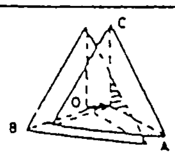
$Z_{1,2.3}$	INSIDE TRIHEDRON OA, OB, OC	–	1,2 & 3	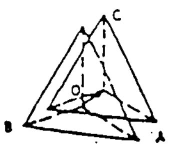

Figure 5 Types of rupture governed by the direction of the resultant of the applied forces (Londe et al., 1969).

In general, these previous studies were related to the possible modes of failure due to the direction of the resultant $\vec{R}$ of the applied forces acting on the rock block, and assuming conservatively that the shear strength along the contact planes is only due to friction.

Years later, with the development of better computational systems, more complex analyses combining vector and graphical methods were made by Goodman (1980), Hoek and Bray (1981), Goodman and Shi (1985), Warburton (1993), and Priest (1993) among others. These analyses were mainly based on information taken from the contributions made by the authors previously mentioned. For instance, much of the work made on the stability analysis of wedge failures by Wittke was enhanced to take into account a few relevant parameters that depend on the dimensions of the rock block. Parameters as the area of sliding faces, blocks volume and position of the block's center of mass were included in the vector analysis that was developed by Goodman (1980), and Hoek and Bray (1981).

Goodman and Shi (1985) developed a geometric approach for excavations in hard jointed rock called *block theory*. The theory behind this geometric approach is based on geological information such as the orientation and properties of the joints into the rock mass. This approach permits the determination of the removability and non-removability of dangerous blocks, which are called keyblocks, defined by the intersection of discontinuities and excavation surfaces on rock slopes or underground excavations.

Three important boundary conditions used in the mathematical definition of the problem are:

(a) The constraints imposed by the fixed faces initially in contact with the rock mass.

(b) The direction of the resultant force acting on the block of rock.

(c) The magnitudes of the friction angles on the faces.

Figure 6 shows the six different types of rock blocks that can be described with this concept. They are known with the following names: I key blocks; II potential keyblocks; III safe removable block; IV tapered block; V infinite block; and VI joint block (Goodman, 1989).

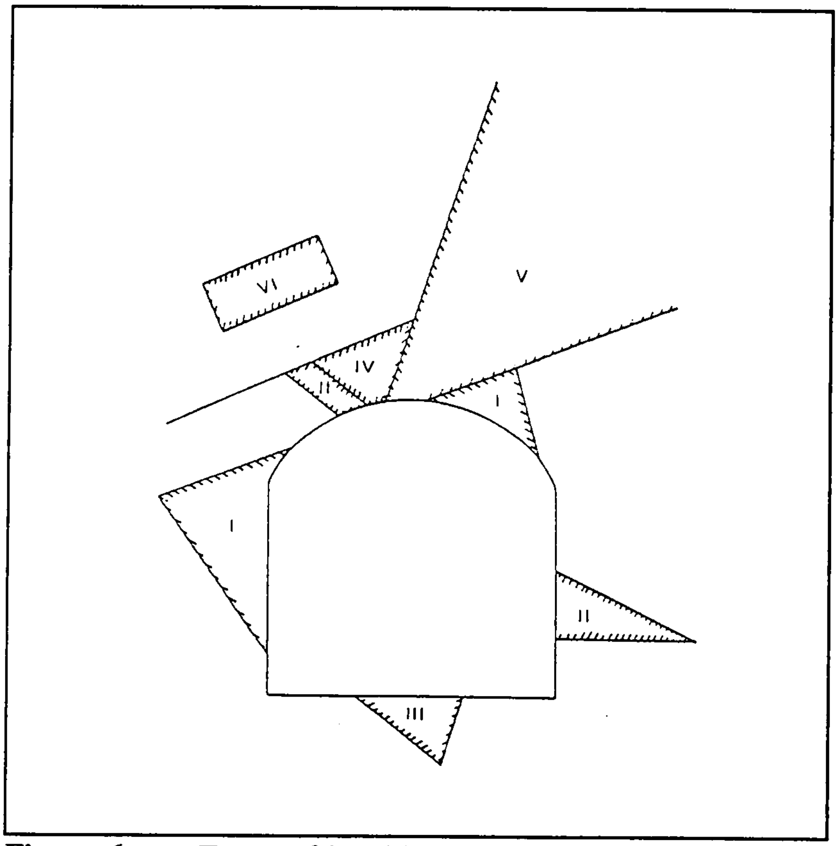

Figure 6 Types of key blocks (Goodman, 1989).

Actually, block theory has been extended to take into account the effect of rotation as a failure mode. The latter studies about edge-rotation modes have been done by Mauldon and Goodman (1990 and 1991) and Mauldon (1992). These studies establish a relationship between the direction of the active resultant force, which for rotational motion may be due to gravity, forces transmitted from adjacent rock masses, seepage forces or external water pressures, and the specific mode of failure, i.e. rotation about an axis along a free edge of the block. Description of these possible failure modes involving rotation of rock blocks is depicted in Figure 7 (Mauldon, 1992).

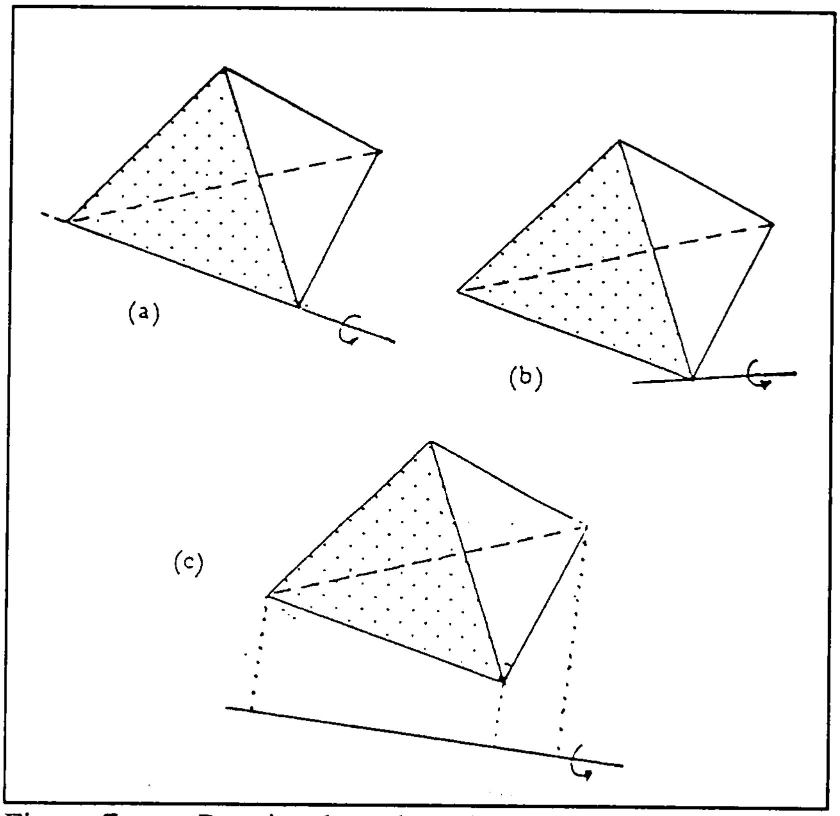

Figure 7 Rotational modes: a) edge rotation, b) corner rotation, and c) remote axis rotation (Mauldon, 1992).

In summary during the early eighties, more and better methods combining vector and graphical methods in two and three dimensions with respect to the problem of slope stability analysis were developed. These studies included new parameters such as the dimensions of the rock block, area of the failure planes, volume of the rock mass, position of the gravity center of mass, and basic geological information such as the orientation and properties of the joints into the rock mass. A particular result of these studies was the development of a new geometric approach for excavations known as *block theory* (Goodman and Shi, 1985). The work presented in this thesis is an extension of block theory for the case of prismatic blocks.

CHAPTER 3

SLIDING STABILITY OF PRISMATIC BLOCKS

3.1 Introduction

In Chapter 1, a prismatic rock block was defined as a rock block bounded by a number *n* of contact planes with the lines of intersection all parallel. The planes of this rock block would constitute a *zone* with a direction parallel to the *zone axis* or line of intersection. Also, if the number of planes tends to infinity ($n \to \infty$), a cylindrical surface is formed as in cylindrically-folded rocks. The normals of all these planes that constitute the *zone* are contained in a great circle and the *zone axis* is defined by the point of intersection of all these great circles on the stereographic projection. Figure 8 depicts the latter condition for a prismatic rock block of four planes whose normals are contained in the great circle #5.

Figure 9 shows a special case of prismatic block which has three planes of contact with the rock mass and lines of intersection all parallel. Furthermore, in Figure 9 a three-dimensional system of coordinates is defined: the *X* axis to the east, the *Y* axis to the north, and the *Z* axis upward (Hendron et al., 1971; Goodman, 1989). This coordinate system is the same assumed to develop the stability analysis in folded rocks using a computer program that is explained in section 3.4. In this chapter an analytical model for sliding stability analysis of prismatic blocks in rock slopes is developed to predict a factor of safety against sliding as a function of friction angles, block geometry, and loading.

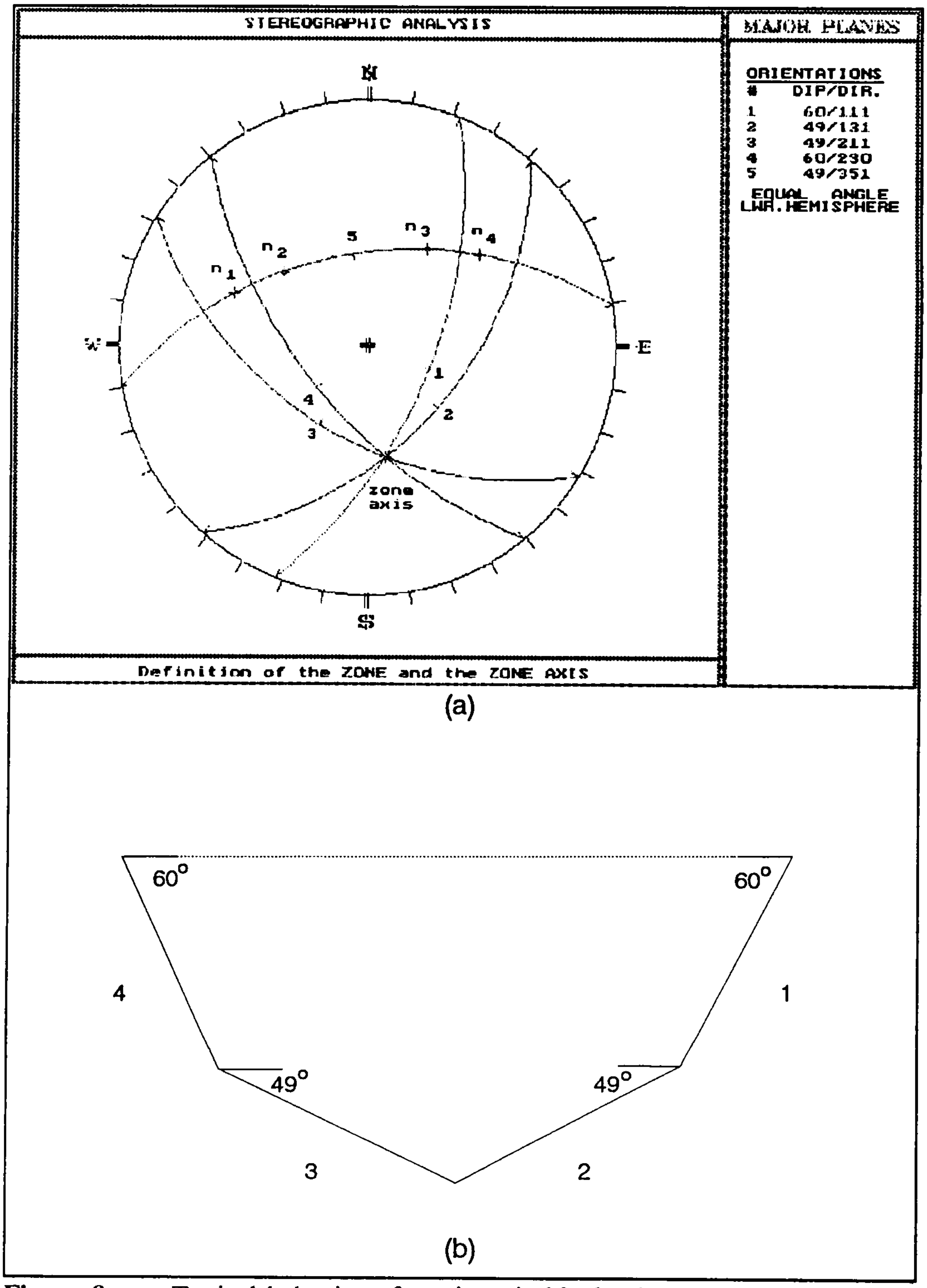

Figure 8 Typical behavior of a prismatic block: a) stereographic projection of the *zone* and *zone axis*; and b) plot of the prismatic block indicating the dips.

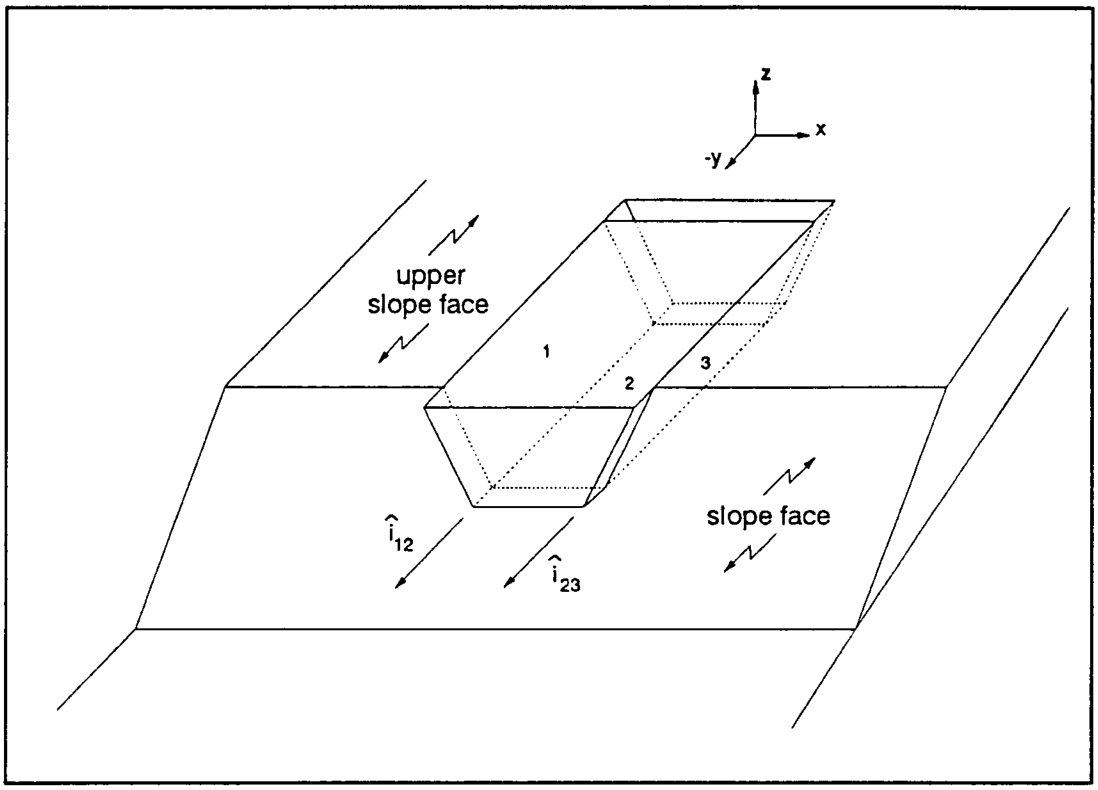

Figure 9 View of a prismatic rock block with three planes of discontinuities.

The stability analysis was simplified to enable the use of block theory. The assumptions used in the simplification are the following:

(a) Unexposed faces of the prismatic rock block are assumed to be planar.

(b) The displacement of the prismatic rock block is due to translation only.

(c) Frictional shear stresses are acting parallel to the sliding direction.

(d) The rock block is undeformable.

(e) The rock block is acted on by an active resultant $\vec{R}$. In the simple case $\vec{R}$ is the weight of the rock block, but may indeed include hydraulic forces, seismic forces, or supporting forces due to anchor bolts.

(f) There is a condition of no rotation in the XZ plane.

The friction force along each contact plane depends on the magnitudes of the normal reaction and the friction angle. If there are three or more contact faces, the distribution of normal forces on those planes is statically indeterminate. If the orientation of the active resultant is such that the block will tend to move parallel to the line of intersection, the stability with respect to sliding is also indeterminate.

To solve this problem one independent approache to determining a safety factor for sliding of prismatic blocks was adopted as follows:

(a) Assume an elastic, conservative system to obtain the distribution of normal forces that minimizes the potential energy of the system.

For the approach in (a), the elastic model of the prismatic block is assumed to be supported at each face by a series of springs, each with stiffness k_i, and each spring initially subject to a "no tension" condition. The elastic model for the prismatic rock block is depicted in Figure 10. Henceforth, this model is generalized to the case of curved failure surfaces as are found in cylindrically folded rocks.

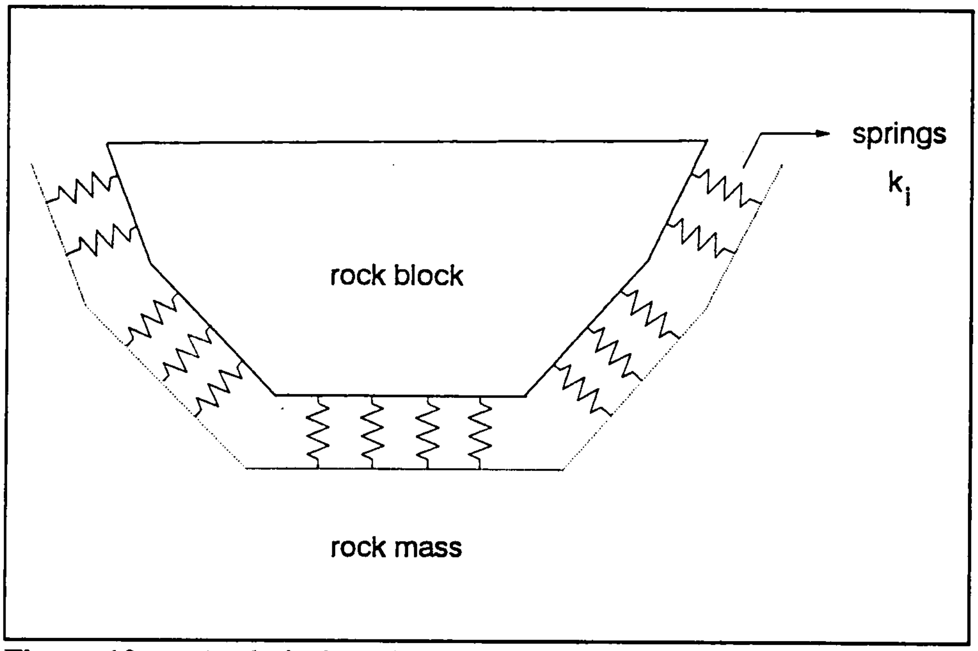

Figure 10 Analytical model assumed to describe the behavior of prismatic rock blocks.

3.2 Mathematical Definition Of The Problem

In a conservative system, the total potential energy is defined as the potential energy stored in the system due to the internal forces and the gravitational potential energy, with respect to a datum, due to the external forces. Therefore the total potential energy of a system consisting of a prismatic rock block supported by m planes of discontinuity is given by:

$$V = V_1 + V_2 + \ldots.. + V_m - W_r = \sum_{i=1}^{m} V_i - W_r \tag{1}$$

where V_i , i = 1,2,...., m planes, is the potential energy of each discontinuity surface, and W_r is the work done by the active forces acting on the rock block. Also, the initial position (datum) was defined such that all spring supports are uncompressed. The potential energy V_i associated with each discontinuity surface is given by:

$$V_i = \int_0^x F\,dx = \int_0^x kx\,dx = \tfrac{1}{2}kx^2$$

where k is the stiffness and x the change in length of the spring. However, to ensure no tension at a displacement of the block , a virtual displacement given by a vector $\vec{s}$ in the plane perpendicular to the line of intersection was assumed, with V_i defined as:

$$V_i = \begin{cases} \tfrac{1}{2}k_i(\hat{n}_i \cdot \vec{s})^2 & if \ (\hat{n}_i \cdot \vec{s}) > 0 \\ 0 & if \ (\hat{n}_i \cdot \vec{s}) \leq 0 \end{cases} \qquad (2)$$

Thus, for any virtual displacement $\vec{s}$ at an angle θ_s and with magnitude s, a set A is defined as,

$$A = A(\theta_s) = \{i : \hat{n}_i \cdot \vec{s} > 0, i = 1,2,...,m\} \qquad (3)$$

This set A is a function of the angle of displacement θ_s ranging from 0 to 180°. It includes discontinuity planes for which the discontinuity surface remains in contact with the rock mass. This will occur only if the condition $\hat{n} \cdot \vec{s} > 0$ is satisfied.

At this point, a number of terms used in the development of the new approach need to be defined as follows:

(a) k_i is the stiffness of plane i.

(b) s is the magnitude of a virtual displacement (assumed small) directed into the rock mass of the rigid block in the direction perpendicular to the incipient sliding direction.

(c) θ_s is the angle defining the direction of the virtual displacement.

(d) $\hat{n}_i$ is the unit normal vector for each discontinuity plane.

(e) θ_i is the angle of each plane measure from the positive X axis.

(f) L_i is the length of each discontinuity plane.

(g) θ_r is the angle defining the direction of the resultant force.

(h) $\vec{R}$ is the resultant of the active forces acting on the rock block. $\vec{R}$ has components perpendicular and parallel to the sliding direction $\vec{R}_N$ and $\vec{R}_T$, respectively.

(i) $\vec{I}$ is the line of intersection between the discontinuity planes.

(j) $\hat{i}$ is the unit vector in the direction of the line of intersection $\vec{I}$.

The variables defined in points (a), (b), and (c) are initially unknown and depend on the results from the new energy-based approach. The variables defined in points (g) and (h) are known from the loading conditions on the slope that affect the stability of the block, and the variables defined in points (d), (e), (f), (i), and (j) are known and depend on the block geometry.

From the conditions mentioned earlier and with all springs acting in compression, equation (1) can be written as a function of the dot product between the displacement and the unit vector of each plane and the component of the active resultant force $\vec{R}_N$ acting in a plane perpendicular to the line of intersection. Thus the potential energy of the system depends on the contact between the planes and the rock mass when θ_s is changing from 0 to 180° according to the following equation:

$$V = \sum_{i \in A} \tfrac{1}{2} k_i (\hat{n}_i \cdot \vec{s})^2 - \vec{R}_N \cdot \vec{s} \tag{4}$$

The dot product $\hat{n}_i \cdot \vec{s}$, that is the projection of the virtual displacement on the unit vector, $\hat{n}_i$, can be replaced by the components and angles between the virtual displacement vector and the unit normal vector for each plane giving the following result,

$$V = \sum_{i \in A} \tfrac{1}{2} k_i s^2 \cos^2(\theta_s - \theta_i) - R_N \, s \cos(\theta_s - \theta_r) \tag{5}$$

where R_N and s are magnitudes.

3.2.1 Equilibrium Condition

The system we have described has two degrees of freedom, θ_s and s. The equilibrium condition is one for what the total potential energy V of the system is stationary. Thus, for the equilibrium condition we have the requirements:

$$\frac{\partial V}{\partial \theta_s} = 0 \quad and \quad \frac{\partial V}{\partial s} = 0$$

The first step is to take the partial derivative with respect to θ_s, while keeping s constant:

$$\frac{\partial V}{\partial \theta_s} = \frac{\partial}{\partial \theta_s}\left(\sum_{i \in A} \tfrac{1}{2} k_i s^2 \cos^2(\theta_s - \theta_i) - R_N \, s \cos(\theta_s - \theta_r)\right) \tag{6}$$

It is noted that although the set A changes with θ_s, the function is piecewise continuous. The derivative of the above expression gives:

$$\frac{\partial V}{\partial \theta_s} = \sum_{i \in A} (-k_i) s^2 \cos(\theta_s - \theta_i) \sin(\theta_s - \theta_i) + R_N \, s \sin(\theta_s - \theta_r) \tag{7}$$

Equating the above expression to zero yields:

$$\frac{\partial V}{\partial \theta_s} = \sum_{i \in A} (-k_i) s^2 \cos(\theta_s - \theta_i) \sin(\theta_s - \theta_i) + R_N \, s \sin(\theta_s - \theta_r) = 0 \tag{8}$$

For the equation above, the set A is defined for any given value of θ_s.

The second step is to calculate the partial derivative with respect to the displacement, s, while keeping the angle θ_s constant:

$$\frac{\partial V}{\partial s} = \frac{\partial}{\partial s} \left(\sum_{i \in A} \tfrac{1}{2} k_i s^2 \cos^2(\theta_s - \theta_i) - R_N \, s \cos(\theta_s - \theta_r) \right) \tag{9}$$

the result of this derivative is:

$$\frac{\partial V}{\partial s} = \sum_{i \in A} k_i s \cos^2(\theta_s - \theta_i) - R_N \cos(\theta_s - \theta_r) \tag{10}$$

Equating the above expression to zero yields:

$$\frac{\partial V}{\partial s} = \sum_{i \in A} k_i s \cos^2(\theta_s - \theta_i) - R_N \cos(\theta_s - \theta_r) = 0 \tag{11}$$

For the moment we assume that each k_i is known. Now we have two equations (8) and (11) with two unknowns, θ_s and s. Let $\theta_s = \theta_s{}^*$ and $s = s^*$ be the solutions for equations (8) and (11). Now we can express s^* as two different equations as,

$$s^* = \frac{R_N \sin(\theta_s{}^* - \theta_r)}{\sum_{i \in A} k_i \sin(\theta_s{}^* - \theta_i)\cos(\theta_s{}^* - \theta_i)} \tag{12}$$

and,

$$s^* = \frac{R_N \cos(\theta_s{}^* - \theta_r)}{\sum_{i \in A} k_i \cos^2(\theta_s{}^* - \theta_i)} \tag{13}$$

With these two equations of s^* (12) and (13), we can define the magnitude of the angle $\theta_s{}^*$ independently of the displacement s^*. To take this approach both equations are combined and solved in the next step as follows:

$$\frac{R_N \sin(\theta_s{}^* - \theta_r)}{\sum_{i \in A} k_i \sin(\theta_s{}^* - \theta_i)\cos(\theta_s{}^* - \theta_i)} = \frac{R_N \cos(\theta_s{}^* - \theta_r)}{\sum_{i \in A} k_i \cos^2(\theta_s{}^* - \theta_i)} \tag{14}$$

then by clustering terms, and dividing by R_N:

$$\frac{\sin(\theta_s{}^* - \theta_r)}{\cos(\theta_s{}^* - \theta_r)} = \frac{\sum_{i \in A} k_i \sin(\theta_s{}^* - \theta_i)\cos(\theta_s{}^* - \theta_i)}{\sum_{i \in A} k_i \cos^2(\theta_s{}^* - \theta_i)} \tag{15}$$

This equation can be simplified producing the result:

$$\tan(\theta_s^* - \theta_r) = \frac{\sum\limits_{i \in A} k_i \sin(\theta_s^* - \theta_i)\cos(\theta_s^* - \theta_i)}{\sum\limits_{i \in A} k_i \cos^2(\theta_s^* - \theta_i)} \tag{16}$$

This trigonometric equation represents the general solution for prismatic blocks tending to slide parallel to the line of intersection. The value of θ_s* which satisfies this equation is the direction of the virtual displacement of the block center of mass, perpendicular to the sliding direction, which produces the equilibrium condition. At this point, it is regarded that the potential energy of the system will be minimum. However, the equation includes the unknown spring constants k_i. This is discussed in the next section.

3.3 Spring Constant k_i

In the elastic model we assume that the spring constant k_i for each contact plane is proportional to the contact area and therefore, due to the prismatic shape, to the length L of a planar contact in the XY plane. This assumption is reasonable given the behavior of springs in parallel: two parallel springs each with a stiffness k yield an effective stiffness of $2k$. If the spring constants are replaced in equation (16) by the product of the constants $(c)(L_i)$, where the constant c is the constant of proportionality, and L_i is the length of plane i perpendicular to R_T, the magnitude c can be cancelled. Replacing this product in equation (16):

$$\tan(\theta_s^* - \theta_r) = \frac{\sum_{i \in A} c\, L_i \sin(\theta_s^* - \theta_i)\cos(\theta_s^* - \theta_i)}{\sum_{i \in A} c\, L_i \cos^2(\theta_s^* - \theta_i)} \tag{17}$$

factoring and cancelling c,

$$\tan(\theta_s^* - \theta_r) = \frac{\sum_{i \in A} L_i \sin(\theta_s^* - \theta_i)\cos(\theta_s^* - \theta_i)}{\sum_{i \in A} L_i \cos^2(\theta_s^* - \theta_i)} \tag{18}$$

which yields a relationship independent of k_i.

To obtain the value of θ_s* a computer program was used. From equation (18) we define a function $F(\theta_s*)$ as follows:

$$F(\theta_s^*) = \frac{\sum_{i \in A} L_i \sin(\theta_s^* - \theta_i)\cos(\theta_s^* - \theta_i)}{\sum_{i \in A} L_i \cos^2(\theta_s^* - \theta_i)} - \tan(\theta_s^* - \theta_r) \tag{19}$$

We then find the value of θ_s* for which $F(\theta_s*) = 0$. To get the value of θ_s*, the input data required for the computer program are the angles θ_i and the lengths L_i of the m planes of discontinuity, the friction angle, and the angle of the resultant force, θ_r. The computer program can then evaluate equation (19) by varying the angle θ_s* from 0 to 180° as was previously defined for the set A. The result from this equation can be plotted to show how the potential energy changes and reaches a minimum at a specific value of θ_s*. Figure 11 shows the determination of θ_s* for the minimum potential energy of the two-plane rock block example developed in section 3.4.1.1.

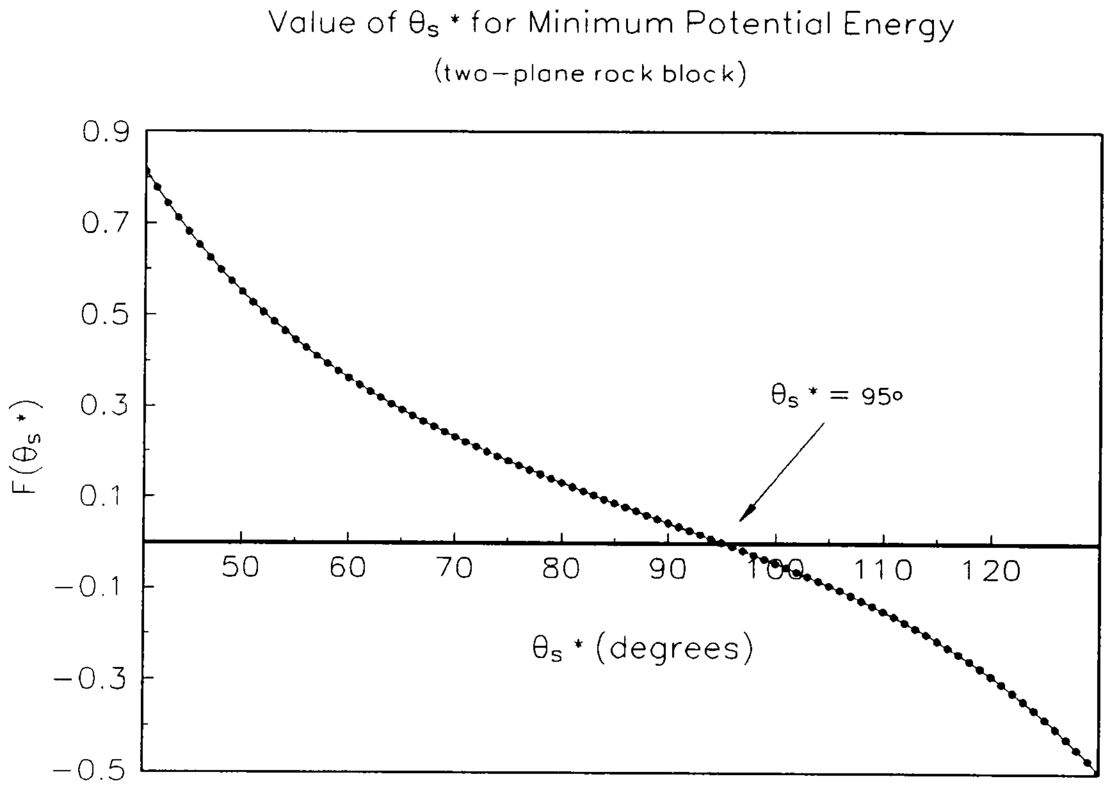

Figure 11 The angle for minimum potential energy θ_s* corresponds to a value of $F(\theta_s*) = 0$.

3.3.1 Determination Of The Normal Forces

With θ_s* known, the magnitude of the displacement, $s*$, for the minimum potential energy can be defined, either using equation (12) or equation (13). The magnitude of $\vec{s}*$ gives the magnitude of a virtual displacement s.

Replacing k_i by $(c)(L_i)$ in equation (13), we obtain:

$$s^* = \frac{R_N}{c} \frac{\cos(\theta_s^* - \theta_r)}{\sum_{i \in A} L_i \cos^2(\theta_s^* - \theta_i)} \tag{20}$$

The magnitude of the normal force for each discontinuous surface due to the small displacement, $\vec{s}\,*$, along the plane, is computed as:

$$N_i = k_i\,(\hat{n}_i \cdot \vec{s}\,^*) \tag{21}$$

or, remembering the definition of k_i,

$$N_i = c\,L_i\,(\hat{n}_i \cdot \vec{s}\,^*) \tag{22}$$

and replacing the dot product $\hat{n}_i \cdot \vec{s}\,*$,

$$N_i = c\,L_i\,(s^*)\cos(\theta_s{}^* - \theta_i) \tag{23}$$

where N_i is finally defined as,

$$N_i = c\,s^*\,L_i \cos(\theta_s^* - \theta_i) \tag{24}$$

This is the general equation to calculate the normal force acting on each plane that must be evaluated using a computer program (see Figure 12).

Using equation (24), the friction force can also be evaluated for each plane of discontinuity with different angles of friction ϕ_i as:

$$F_i = N_i \tan\phi_i \tag{25}$$

replacing N_i,

$$F_i = \tan\phi_i\;[c\,s^*\,L_i \cos(\theta_s{}^* - \theta_i)] \tag{26}$$

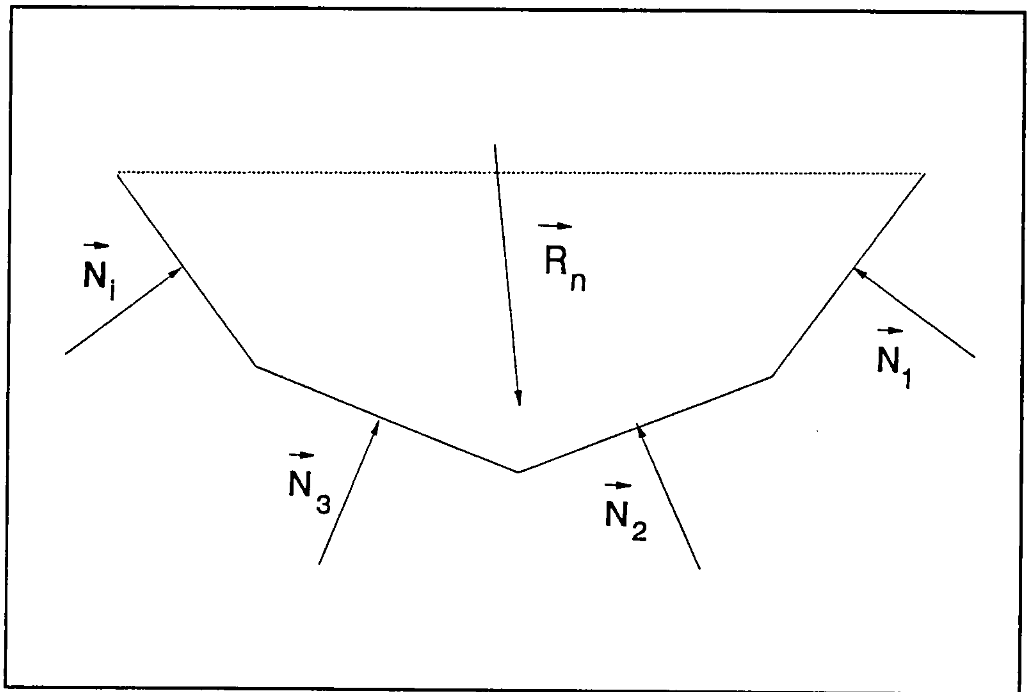

Figure 12 Distribution of normal forces as defined by equation 24.

In this way the safety factor for prismatic blocks, assuming that sliding is resisted by friction only and that the friction angle ϕ_i is the same for each plane, is evaluated as the summation of all friction forces (total resisting force) acting on the discontinuous surfaces divided by the component of the active resultant force (driving force) acting in a plane parallel to the line of intersection. To begin with the evaluation of the safety factor, equation (26) must be expressed as a summation in the following manner, (where we assume the friction angle is the same for each plane),

$$\sum_{i=1}^{n} F_i = \tan\phi \; c\, s^* \sum_{i \in A} L_i \cos(\theta_s^* - \theta_i) \tag{27}$$

substituting s^* from equation (13),

$$\sum_{i=1}^{n} F_i = c \tan\phi \left[\frac{R_N}{c} \frac{\cos(\theta_s^* - \theta_r)}{\sum_{i \in A} L_i \cos^2(\theta_s^* - \theta_i)} \right] \sum_{i \in A} L_i \cos(\theta_s^* - \theta_i) \tag{28}$$

simplifying terms,

$$\sum_{i=1}^{n} F_i = R_N \tan\phi \cos(\theta_s^* - \theta_r) \frac{\sum_{i \in A} L_i \cos(\theta_s^* - \theta_i)}{\sum_{i \in A} L_i \cos^2(\theta_s^* - \theta_i)} \tag{29}$$

where, $A = \{i : \hat{n}_i \cdot \vec{s} > 0,\ i = 1,2,\ldots,m\}$

Equation (29) represents the total resisting force against sliding for the discontinuous surfaces of a rock block. Now, with this solution, the safety factor can be expressed as:

$$FS = \frac{TOTAL\ RESISTING\ FORCE}{DRIVING\ FORCE} \tag{30}$$

where the numerator of equation (30) is the term defined in equation (29) as the summation of all friction forces, and the denominator is R_T or the component of the active resultant force acting parallel to the line of intersection defined by the unit vector $\hat{i}$.

The safety factor is then defined as follows:

$$FS = \frac{R_N \tan\phi \cos(\theta_s^* - \theta_r) \dfrac{\sum\limits_{i\in A} L_i \cos(\theta_s^* - \theta_i)}{\sum\limits_{i\in A} L_i \cos^2(\theta_s^* - \theta_i)}}{R_T} \tag{31}$$

replacing R_N and R_T by ($R\ sin\ \delta$) and ($R\ cos\ \delta$), respectively, the magnitude of R cancels out, so that the final result is:

$$FS = \tan\phi \tan\delta \cos(\theta_s^* - \theta_r) \frac{\sum\limits_{i\in A} L_i \cos(\theta_s^* - \theta_i)}{\sum\limits_{i\in A} L_i \cos^2(\theta_s^* - \theta_i)} \tag{32}$$

where, $A = \{i : \hat{n}_i \cdot \vec{s} > 0,\ i = 1,2,\ldots,m\}$

and δ is the angle between the resultant $\vec{R}$ and the unit vector $\hat{i}$ (see Figure 14).

Equation (32) is a dimensionless ratio because it does not depend on the magnitude of the resultant force R. Equation (32) is just defined by the direction of the resultant force θ_r, the direction of each discontinuity plane θ_i, and the direction of the virtual displacement θ_s*, perpendicular to the sliding direction, which produces the equilibrium condition .

The next section deals with the evaluation of different models using the computer program. The problems were solved using the concept of potential energy previously developed in this chapter. The main goal is to determine the safety factor with respect to translational slip of a prismatic block formed in a rock slope by the intersection of discontinuities with parallel lines of intersection.

3.4 Analytical Models

The model for the stability of prismatic blocks was implemented in a computer program. The following is a general description of the assumptions made within this computer program in addition to those previously stated in section 3.1:

(a) No shear stress is acting along the plane perpendicular to the line of intersection,

(b) The active resultant force acting on the blocks is due to gravity alone,

(c) The friction angle is the same for each plane,

(d) The length of each plane L_i is obtained from field data. As was mentioned before the effect of the length is related to the stiffness k_i of each plane. This is very important because this parameter has a direct influence on the magnitude of the normal force acting on each plane.

(e) There is no restriction on the inclination of the crest of the slope, and in the model, pore pressure and tension crack are not included in the analysis.

Some of the variables defined in section 3.2 such as θ_i, L_i, and $\hat{n}_i$ are depicted in Figure 13, as part of the input data used by the computer program.

The following is a brief description of the computer program. A three-dimensional system of coordinates was assumed with the X axis to the east, the Y axis to the north, and the Z axis upward. The computer program starts by asking for the dip and dip direction of each plane, the direction of the resultant, the friction angle value,

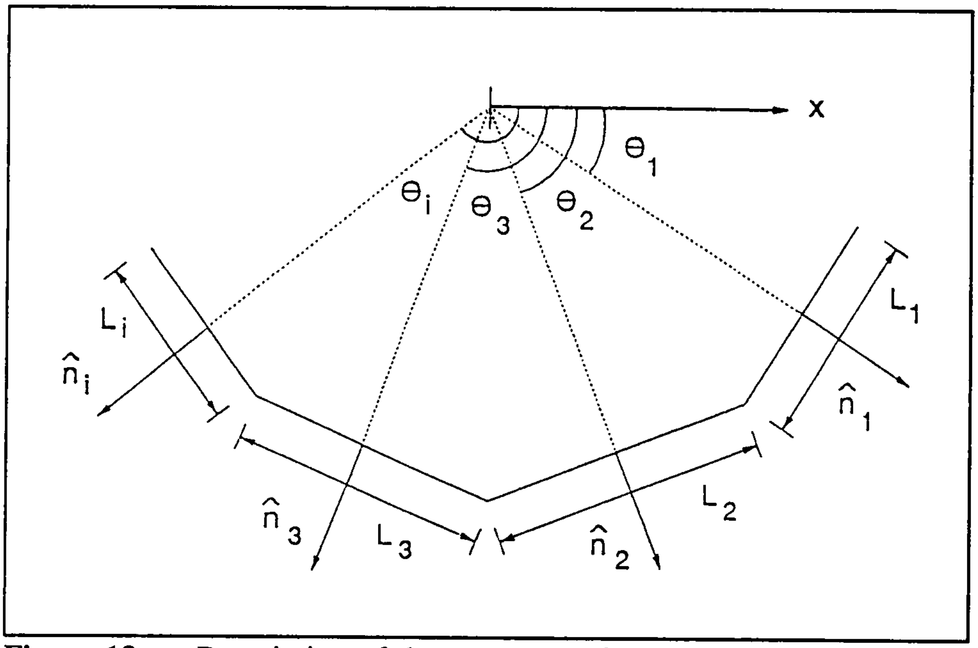

Figure 13 Description of the geometry of prismatic blocks used by the computer program

the angle from the X direction, and the length of each plane. All data can be edited in one input file. The next step is to get the component of the result parallel and normal to the line of intersection called R_N and R_T (see Figure 14). Also it is possible to verify, doing the dot product on every two planes, that the lines of intersection are parallel. Using equation (19), we get the angle θ_s* for which the potential energy is assumed to be minimum. The magnitude of this angle is then used in equation (29) along with the magnitude of R_N, to obtain the summation of friction forces acting on the prismatic block.

The final step is the evaluation of the factor of safety using equation (32). The computer program uses equations (13), (19), (24), and (29) directly to give an output file with the required information for further calculations. This output file can be retrieved using a file editor. A solution for some cases as two- and three-plane wedges are

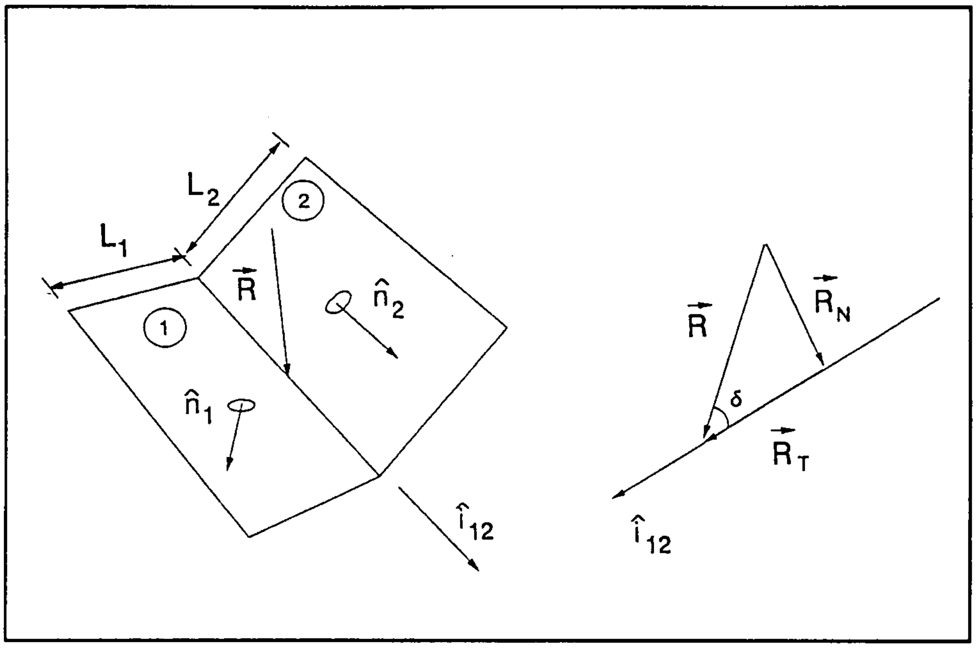

Figure 14 Two-plane prismatic block used for analytical analysis.

presented next to show the procedure used in the solution of the models. The result can be verified by hand using the equations mentioned before.

3.4.1 Description of the Two-Plane Prismatic Block (Rock Wedge)

Figure 14 provides a general description of a two-plane block as it is used in this example. Using equation (19) for a specific value of θ_s* some of the planes may not be in contact with the surrounding rock mass. The assumptions made at the beginning of the section, i.e., no shear stress is acting perpendicular to sliding direction, still apply. Thus the equilibrium equations, $\Sigma F_x = 0$ *and* $\Sigma F_y = 0$, are satisfied and the system is statically determinate. Let us start with the definition of the variables used in this analytical solution.

The failure surfaces in Figure 14 are denoted by 1 and 2. The following input data are required for the solution of the problem:

(a) ψ_i, α_i = dip and dip direction of the discontinuity planes

(b) ϕ = angle of friction assumed equal for both planes

(c) L_i = length of each plane

(d) θ_i = angle of each plane measured from the positive X axis

(e) m = number of planes

Other terms used in the solution are:

(f) FS = factor of safety against sliding along the line of intersection

(g) R_N = component of the resultant perpendicular to the line of intersection

(h) R_T = component of the resultant parallel to the line of intersection

(i) s* = small displacement of the block corresponding to minimum potential energy.

(j) θ_r = angle of R_N measured from the positive X axis

(k) θ_s* = angle for which the minimum potential energy is reached

(l) $\vec{I}_{12}$ = line of intersection between planes 1 and 2

(m) $\hat{i}_{12}$ = unit vector in the direction of the line of intersection $\vec{I}_{12}$

(n) N_i = magnitude of normal force on each plane.

3.4.1.1 **Example**

This example is developed initially for a two-plane rock block with lengths of planes defined by the ratio $L_1/L_2 = 1$ and active resultant force due to gravity alone. This is the classic wedge failure problem (Hoek and Bray, 1981) and is included here as validation of the proposed model, since the two-plane rock block is statically determinate. To calculate the factor of safety, dip and dip directions of planes 1 and 2 are required, so that the following data apply:

Plane	1	2
$\psi°$	30°	40°
$\alpha°$	85°	235°
$\phi°$	20°	20°

Note that as L is equal for both planes, it will cancel out itself, so that for this calculation it is not required to know its magnitude.

The calculation of the different values is as follows:

(a) Unit normal vectors using the dip and dip direction of planes 1 and 2

$$(n_{1x}, n_{1y}, n_{1z}) = (\sin\psi_1 \sin\alpha_1, \sin\psi_1 \cos\alpha_1, \cos\psi_1)$$

$$= (0.4981, 0.0436, 0.8660)$$

$$(n_{2x}, n_{2y}, n_{2z}) = (\sin\psi_2 \sin\alpha_2, \sin\psi_2 \cos\alpha_2, \cos\psi_2)$$

$$= (-0.5265, -0.3687, 0.7660)$$

(b) The resultant active force acting on the block is due to gravity alone, therefore, $\vec{R} = (0, 0, -W)$. The vector of intersection between planes 1 and 2 is defined by $\hat{i} = (0.3821, -0.9075, -0.1741)$. So that the dot product between the resultant force and the unit vector of the line of intersection is equal to, $(\vec{R} \cdot \hat{i}) = 0.1741 \ W > 0$

(c) Components R_T and R_N of the resultant defined as $[(\vec{R} \cdot \hat{i})\ \hat{i}]$ and $[R - R_T]$, respectively,

$R_T = (0.0665\ W, -0.1580\ W, -0.0303\ W)$; $R_T = |\ 0.1741\ W\ |$

$R_N = (-0.0665\ W, 0.1580\ W, -0.9696\ W)$; $R_N = |\ 0.9847\ W\ |$

(d) From equation (19) with $\theta_1 = 51.07°$ and $\theta_2 = 118.42°$, and lengths $L_1 = L_2 = 1$, we have that the direction is $\theta_s{*} = 95.5°$, and from equation (13), the displacement is $s{*} = 0.73428$.

(e) Using now equations (24) and (29), we can calculate the value of the normal force on each plane and the summation of friction forces (total resisting force), e.g., the plane normals are $N_1 = 0.5163$ W, and $N_2 = 0.6659$ W.

(f) Finally, from equation (32) the safety factor is found to be: FS = 2.4713.

Here, it is not really necessary to know the magnitude of W because as was explained in the definition of equation (32), the factor of safety is independent of the magnitude of the resultant force *R*. The results of this first example agree with the solution for two planes that is calculated using the equilibrium equations defined by Hoek and Bray (1981). A description of the wedge geometry used by Hoek and Bray is depicted in Figure 15. The latter is verified next using the dips of the planes defined in the previous example.

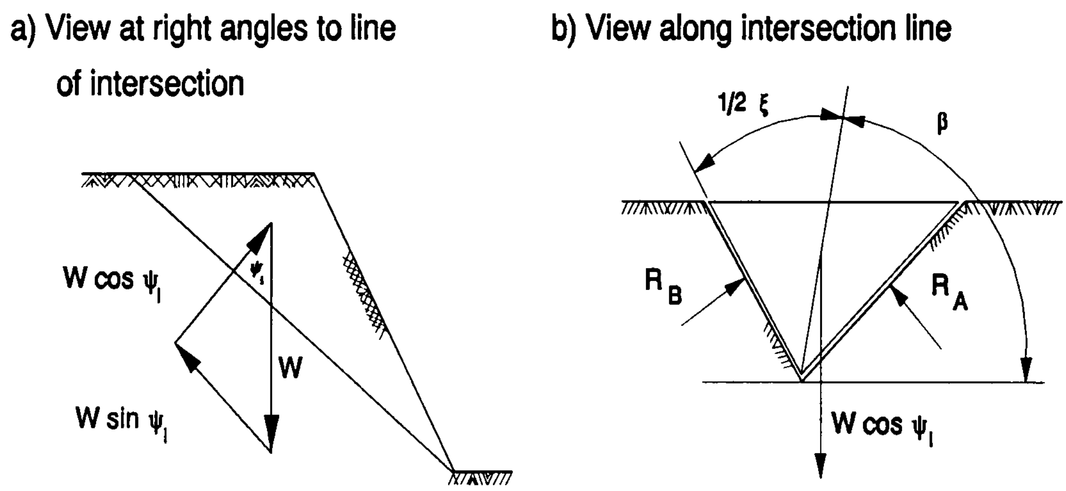

c) Factor of safety:

$$FS = \frac{(R_A + R_B)\tan\phi}{W \sin\psi_i}$$

Figure 15 Definition of wedge geometry (Hoek and Bray, 1981).

Hoek and Bray defined the factor of safety with respect to a wedge failure in the following way:

$$FS = \frac{(R_A + R_B)\tan\phi}{W\sin\psi}$$

where, (a) R_A and R_B are the normal reactions on each plane depending on the weight W of the rock wedge. These values are equal to 0.5078 W and 0.6706 W, respectively;

(b) ϕ is defined as the friction angle and is equal to 20°;

(c) ψ is the plunge of the intersection line of both planes and is equal to 10.03° for this example.

replacing the values we obtain,

$$FS = \frac{W(0.5078 + 0.6706)\tan 20^o}{W\sin 10.03^o} = 2.4621$$

Note that the weight of the rock wedge cancels out in the above equation. The safety factor is equal to 2.4621, which represents a difference of 0.40 % with respect to the result 2.4713 from the analytical model. This difference, which is insignificant, is a consequence of the numerical approximation to the solution of equation (13). The analysis was repeated for the following ratios: $L_1 = 2L_2$ and $L_2 = 2L_1$. In each case the factor of safety remained the same (to 2 significant figures), although the angle of the displacement θ_s* changed. Table 1 summarizes these results as follows:

ratio L_1 : L_2	F.S.	θ_s*
½	2.4582	67°
1	2.4713	95.5°
2	2.4589	117°
Limit Equilibrium	2.4621	

Table 1 Summary of wedge failure analysis using the new mathematical approach.

This example was developed to compare the accuracy of the new energy-based stability analysis with the limiting equilibrium approach described by Hoek and Bray (1981), Goodman (1980), and many other authors. Only in the case of a two-plane block is this direct comparison possible. Having gained some confidence in the new model, we proceed with a three-plane prismatic block which is the next example.

3.4.2 **Description of the Three-Plane Prismatic Block**

As was previously stated at the beginning of the chapter, for a rock block with one or two fixed faces (plane or wedge failure), it is possible to determine that the block will attempt to move either parallel to one of the faces when $\hat{n} \cdot \vec{s} = 0$ or along the line of intersection for both planes when $\vec{R}_T \cdot \vec{s} > 0$. For these conditions, the effect of friction on the fixed faces can be determined by appropriate resolution of forces. For the case in which a rock block has three or more supporting fixed faces, Warburton

(1993) regards that the block will attempt to move guided by the supporting faces whose lines of intersections are parallel. But the solution for such a configuration results in a system of equations that is statically indeterminate when friction force is regarded on each plane. At this point, the new concept regarding the potential energy of the system is of extreme importance because it quickly simplifies the stability analysis of any slope when the rock block is acted on by friction.

Figure 9 shows a general view of a prismatic block with three planes of discontinuities as it was used to develop the example in this section. The parameters and the sequence of calculations defined in the previous section for two planes of discontinuities are the same used in this example, except that, there is now one more plane of discontinuity. However, the analysis for this case is made through graphics to show how the safety factor of the three-plane prismatic block is affected by different boundary conditions. The graphs are based on factors such as the friction angle, lengths of the planes, and plunge and trend of the line of intersection.

The initial data of this example are as follows:

Plane	1	2	3
ψ°	45°	23°	45°
α°	120°	185°	250°

where ψ is the dip and α is the dip direction of each discontinuity plane. The plunge and trend of the intersection line for this example is defined by the dip and dip direction of plane 2.

The first graph is developed assuming four different values of friction angles, and with lengths $L_1 = 1$ and $L_3 = 1$. The length L_2 of the second plane is assumed to change in proportion to the magnitude of either L_1 or L_3. The result of these initial conditions is shown in Figure 16.

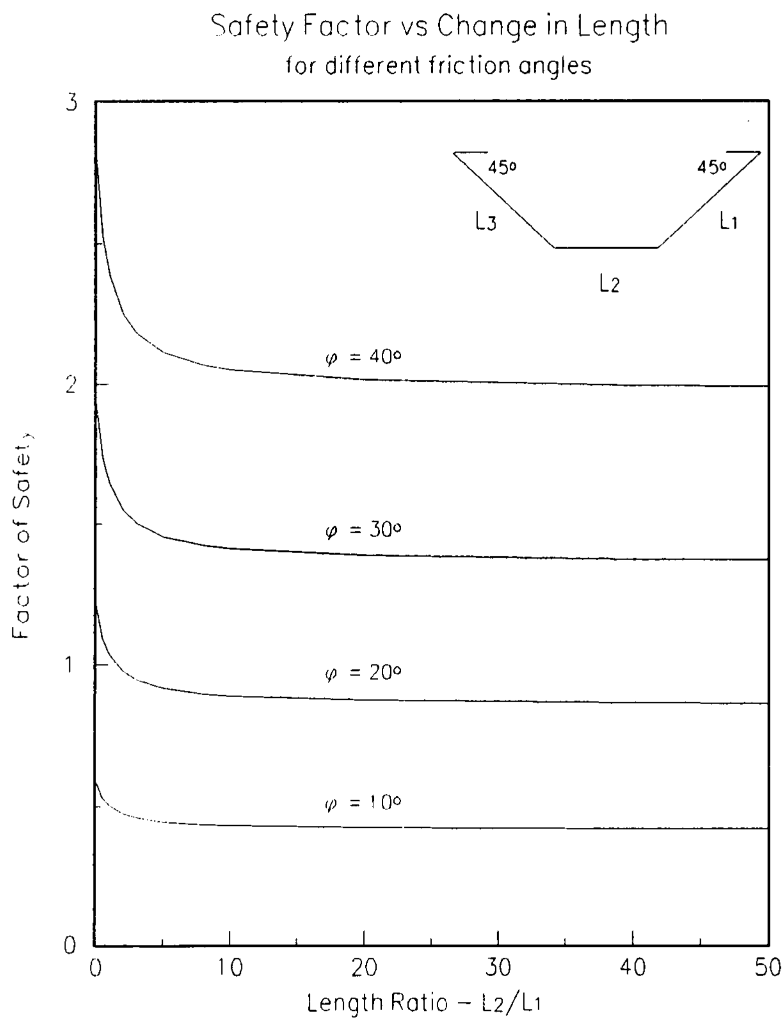

Figure 16 Reduction of the factor of safety with change in the length ratio L_2/L_1.

The main result is that there is a reduction in magnitude of the factor of safety when L_2 increases. Through this graph, it is possible to observe that for a value of L_2 greater than about 25, the factor of safety tends to be constant. Thus, the lower and upper bounds for the geometry of this three-plane prismatic block are found for each value of the friction angle. Figure 17 shows the change of L_2 with more detail for a section taken from Figure 16 when the value of the friction angle is equal to 20°, and the length L_2 ranges from 0 to 5.

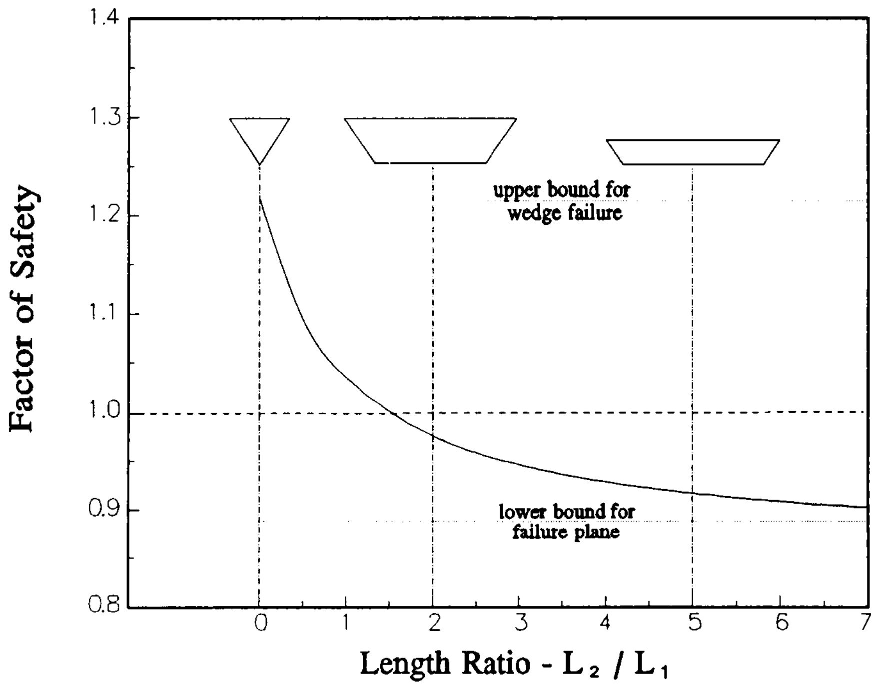

Figure 17 Reduction of the safety factor when the length ratio L_2/L_1 increases for a friction angle of 20°.

The upper bound of the prismatic block corresponds to the case of a wedge failure sliding upon two contact planes in a direction parallel to the line of intersection of the discontinuity planes when $L_2 = 0$ (see Figure 15). The lower bound of the prismatic block corresponds to the simple case of plane failure when L_2 increases in proportion to the lengths L_1 or L_3. The latter condition is explained in the following paragraph (see Figure 18).

For plane failure, Hoek and Bray (1981) and Goodman (1989) define the factor of safety of a failure plane according to the following equation:

$$FS = \frac{\tan \phi}{\tan \psi}$$

where, ϕ = friction angle of the plane,

ψ = dip of the plane.

If the angle ϕ is equal to the angle ψ, the safety factor is one and the slope is on the point of failure. At this point, there is an equilibrium between the forces tending to resist sliding and those forces inducing sliding. This condition is known as limiting equilibrium. For a specific friction angle, a value of ψ greater than ϕ reduces the safety factor less than one and the failure occurs. Thus, the behavior of this prismatic block under these conditions corresponds to the lower bound. In Figure 18 this limit condition for plane failures can be seen.

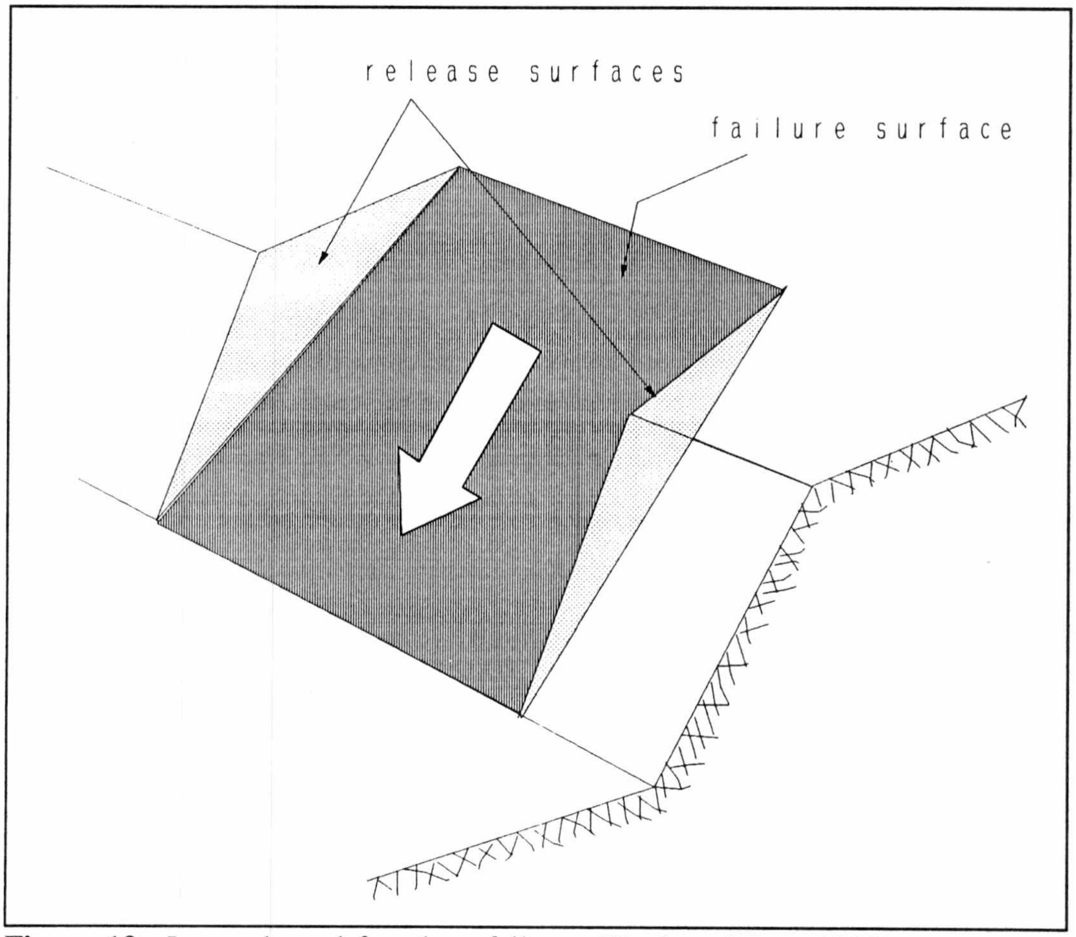

Figure 18 Lower bound for plane failures (Hoek and Bray,1981).

Figure 19 shows the variation in FS with plunge for different values of friction angle. In this graph the trend of the line of intersection is kept constant. For this specific case, the dip of plane 2 is equal to the plunge of the line of intersection. Therefore, the dip of plane 2 changes with the variation in plunge of the line of intersection. This condition produces a change on the dips of the lateral planes 1 and 3 when the plunge of the intersection line ranges from 0 to 90°. The lengths are all equal such that $L_1/L_2 = L_2/L_3 = L_1/L_3 = 1$. As the plunge increases, the factor of safety is reduced, and the failure of the prismatic block is imminent when the magnitude of the friction angle equals the magnitude of the plunge of the intersection line (FS = 1). Beyond that point, sliding of the block occurs.

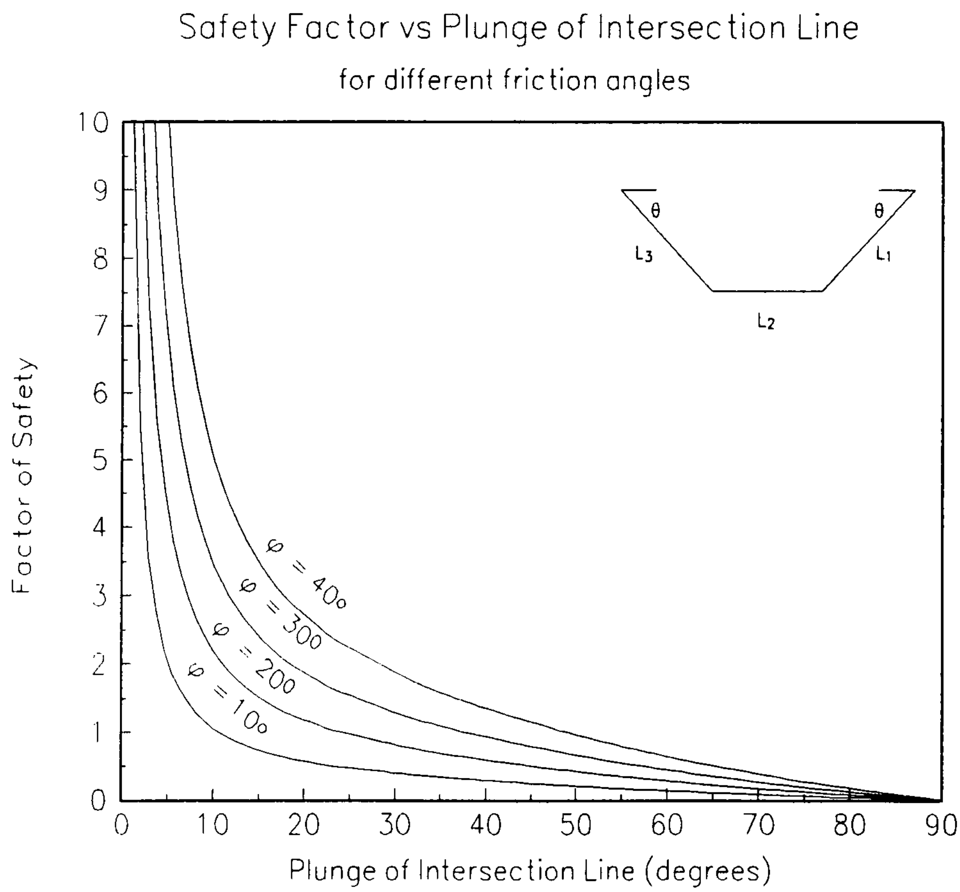

Figure 19 Reduction of the safety factor when the plunge of the intersection line decreases.

In summary, this new mathematical approach taking into account the concept of minimum potential energy allows us to calculate the magnitudes of the normal forces acting on the different discontinuity planes. Thus, the total resisting force of a prismatic block against sliding is known. If the rock block slides, its movement will be parallel to the line of intersection determinated from the intersection of the discontinuity planes. The new energy-based approach was shown to correspond to the classical limit equilibrium method for a wedge failure (upper bound) and plane failure (lower bound). It will now be applied to an actual rock slope.

CHAPTER 4

CASE STUDY FROM EAST TENNESSEE

4.1 Regional Geology

One of the main natural agents in changing Tennessee's landscape over many millions of years has been running water. The effect of water upon the igneous and metamorphic rocks that underlie much of the high mountain ground of East Tennessee has been through the action of weathering and erosion. This resulted in a great variety of geologic features such as plains, hills, ridges, valleys and mountains that can be observed throughout the Valley of East Tennessee and the Unaka Mountains.

The other natural agent that has acted in forming and molding the zone has been the tectonic stresses which produced geologic structures as folds, faults, and joints. The region of the Valley of East Tennessee and the Unaka Mountains have undergone the effects of these disturbing forces causing overturning, overlapping, and lifting of different layers of young and old rocks (rock material from earlier times, i.e. Precambrian and Paleozoic times). The most common result in East Tennessee of these gigantic forces has been thrust faulting (Wilson,1981).

Chilhowee Mountain is the dividing line between the Unaka Mountains and the Valley of East Tennessee. These areas are also known as the Blue Ridge and the Valley and Ridge Provinces, respectively (Tucker, 1951). A description of how these geologic provinces were formed is needed at this point (see Figure 20).

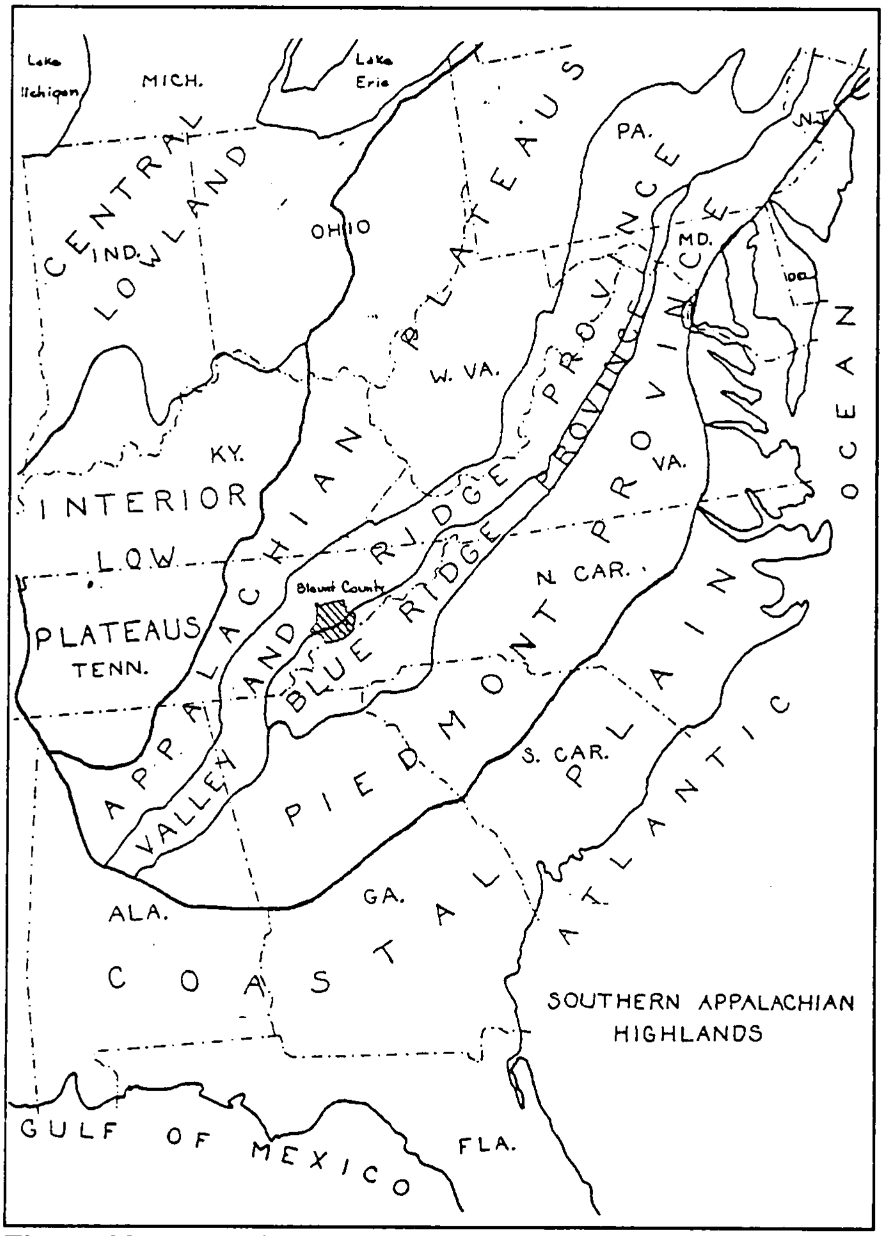

Figure 20 Physiographic divisions eastward of the United States (National Atlas, 1968).

4.1.1 **Unaka Mountains**

Extending parallel to the Tennessee-North Carolina boundary, this geologic province is a mountainous section that lies west of the Piedmont Province and east of the Valley and Ridge Province (see Figure 20). It extends from the Susquehanna river in Pennsylvania where it is approximately 22.5 Km (14 miles) wide, to northern Georgia where it reaches a maximum width of 112.5 Km (70 miles) (Tucker,1951).

The Unakas are underlain by highly weathered metamorphic rocks which are Precambrian in age, and of complex structure, i.e. metasiltstone, metasandstone, and metacongloromerate. There is also a series of early Cambrian sediments and local coves floored by Ordovician limestone and dolomite (Wilson,1981). Another feature that characterizes the Unakas is the high degree of deformed rocks. This condition is more easily appreciated between the Valley and the Unaka division in which folds and dislocations, and consequently, dipping strata are the rule (Safford,1869). The cause of the disturbance that has affected the geology of the whole region are the two thrust faults known as the Greenbrier thrusting and the Great Smoky thrusting. The latter actually forms the northwestern boundary of the region. At many places along this western margin, the Great Smoky fault has brought the Precambrian strata, formed of older rocks, in contact with younger and softer Paleozoic rocks such as limestone, forming coves or windows because of the weathering of the older rocks in these areas. Examples of these windows are found in Miller, Tuckaleechee, Wear, and Cades Cove (Tucker, 1951; Wilson, 1981).

4.1.2 Valley and Ridge of East Tennessee

This region consists of a series of prominent ridges and intervening valleys. It extends northeast-southwest from the St. Lawrence Valley to the Gulf Coastal Plain in Alabama. At its widest point toward the northeast, the Valley and Ridge is about 93 Km (58 miles) wide. Southward it narrows to a width of 53 Km (33 miles). In Tennessee, the province is bounded on the northwest by the Appalachian Plateaus Province and on the southeast by the Unakas (Tucker, 1951; Wilson, 1981).

Sediments of Paleozoic age as limestone, sandstone, and shale form almost all type of rocks of the Valley and Ridge. In most cases, the ridges are supported by resistant sandstones, while the valley floors are made up of less resistant limestones and shales (Safford, 1869; Tucker 1951). With respect to the geological structure, this province can be considered one of the most complex regions of the state. In one period of the earth's history nearly all rocky formations of Tennessee were continuous and relatively horizontal over the whole state. In East Tennessee, these rock formations were compressed, folded and displaced by great disturbing forces (mainly from the Great Smoky thrust) acting in a northwestern direction along the southeastern edge of these horizontal formations. At times, these forces produced pressures so great that the rock strata were ruptured, forming thrust faults (Safford, 1869; Wilson, 1981).

The valleys and ridges are actually the result of differential erosion of these folded strata, which were not all of the same hardness. The ancient anticlines, the result of thrust faulting, were the first to be attacked by the forces of weathering and erosion, and displayed less resistant layers that were very easily eroded into valleys

(Tucker, 1951; Wilson, 1981).

4.2 Geological Formation Of The Study Area

The geological formation of the study area is tightly related to the bedrock geology of the Great Smoky Mountains and their surroundings. Thus, the geologic history, which can be deduced from it, is characterized by three steps as follows (King et al., 1968):

(a) The first step includes the metamorphic and granitic rocks characteristic of the Blue Ridge on the southeast named *the basement complex*. This basement complex consists of a wide variety of gneiss and schists, including both layered gneiss derived from sedimentary or volcanic rocks and non layered, mostly granitic, gneiss representing intrusive bodies. Its age is approximately of earlier Precambrian time (formed more than a billion years ago).

(b) The Ocoee Series represents the second step, and is of later Precambrian time (1 billion to 600 million years ago). This series is formed by pebbly, sandy, and muddy sedimentary rocks which form most of the Great Smoky Mountains and large parts of the adjacent foothills. The series is grouped in several differing parts called the Snowbird, Great Smoky, and Walden Creek Groups. A noteworthy feature of this series is that it has been affected by the two thrust faults mentioned before (see Figure 21).

(c) The sedimentary rocks of the Appalachian Valley represent the third step, and are of Paleozoic time (formed 600 million to 300 million years ago). These sedimentary rocks are divided in three structural groups with different geographical situations, but they have in common the Great Smoky and related thrust sheets. These rocks can be seen on the west (Chilhowee Mountain and Miller Cove) and northwest edge (boundary with the Appalachian Valley) of the foothill belt of the Smoky Mountains. There are also some windows produced by erosion through the Great Smoky thrust sheet where the Paleozoic rocks (limestone of the Ordovician group) can be observed (see Figure 22).

Age	North of and below Greenbrier fault				
Cambrian(?) and Cambrian	Chilhowee Group		Cochran Formation and higher units		
			Disconformity?		
Later Precambrian	Ocoee Series	Walden Creek Group	Sandsuck Formation Wilhite Formation Shields Formation Licklog Formation		
			Fault contact, sequence uncertain		
			Western part of area	Eastern part of area	
		Unclassified formations	Cades Sandstone	Rocks of Webb Mountain and Big Ridge	Rich Butt Sandstone
		Snowbird Group	Metcalf Phyllite	Pigeon Siltstone Roaring Fork Sandstone Longarm Quartzite Wading Branch Formation	
			Base not exposed	Unconformity	
Earlier Precambrian				Basement complex	

Figure 21 Stratigraphic units of the Ocoee Series-Precambrian time (King et al., 1968).

System	Series	Formation or group		Thickness (feet)	Description
Mississippian	Upper	Greasy Cove Formation		400	Limestone, shale, and sandstone.
	Lower	Grainger Formation		1,000	Siltstone, sandstone, and conglomerate.
Devonian	Upper	Chattanooga Shale		25	Thin persistent unit of black carbonaceous shale.
		Unconformity			
Ordovician	Middle	Bays Formation		900	Red calcareous mudrock and siltstone; white sandstone at the top.
		Sevier Formation		2,000	Greenish-gray calcareous shale, sandstone, and calcarenite.
		Chota Formation		700-1,000	Dark-red to reddish-gray quartzose calcarenite.
		Tellico Formation		3,400	Greenish-gray calcareous shale; persistent calcareous sandstone units.
		Blockhouse Shale		400	Dark-gray calcareous shale; nodular limestone at base.
		Lenoir Limestone		100	Dark-gray nodular and light-gray dense limestone; basal conglomerate in places.
		Unconformity			
	Lower	Knox Group		3,100	Gray thick-bedded limestone and dolomite, very cherty in part; divisible into five formations of dolomite and minor limestone in Appalachian Valley; dominantly limestone in cove areas of Great Smoky Mountains foothills.
Cambrian	Upper				
	Middle	Conasauga Group		1,500	Gray, calcareous shale; several limestone formations.
	Lower	Rome Formation		1,000	Mostly red shale adjacent to mountains; includes much siltstone, sandstone and dolomite to the northwest.
		Shady Dolomite		1,200	Gray to dark-gray thick-bedded dolomite.
		Chilhowee Group	Helenmode Formation	200	Glauconitic siltstone and sandstone, calcareous in part.
			Hesse Quartzite	500	White thick-bedded vitreous quartzite.
			Murray Shale	350	Greenish-gray micaceous glauconitic noncalcareous siltstone and fine-grained sandstone.
Cambrian(?)	Lower (?)		Nebo Quartzite	400	White thin- to medium-bedded vitreous quartzite.
			Nichols Shale	600	Greenish-gray micaceous glauconitic noncalcareous siltstone; thin beds of sandstone and quartzite.
			Cochran Formation	1,200	Thick-bedded quartzite and arkosic sandstone, finely conglomeratic in lower part; red silty shale near base in places.
		Disconformity(?)			
Precambrian	Ocoee	Sandsuck Formation of Walden Creek Group			

Figure 22 Paleozoic formations in the vicinity of the Foothills belt of the Unaka Mountains (King et al., 1968).

The geological formation of Chilhowee Mountain northwestward and the adjacent area to the Foothills Parkway southeastward until Kinzel Spring are of our concern because they show a high level of instability due to the folding and weathering conditions of the rocks. The location of the study area in which these formations are located is described in the following section.

4.2.1 Description and Location of The Study Area

Along Highway 73 in Blount County, Tennessee, between the towns of Walland (mile 23) and Kinzel Springs (mile 29), six mayor rock cuts were identified displaying problems of instability such as rockslides, rockfalls, and dip slope failure among others. A great variety of lithologies are found in these rock cuts ranging from shales and siltstones to distinctive conglomerates formed mostly of large rounded white quartz pebbles, with minor amounts of pebbles of black quartzite, granite, limestone, and many other types of rocks (King et al., 1968). The explanation for this large variety of rock formations inside this small area is the folding and the faulting of the bedrock layers formed by sedimentary rocks from the Precambrian and the Paleozoic period (more than a billion to 300 million years ago).

Figure 23 shows the six rock cuts mentioned above numbered from 1 to 6 on a map section taken from the Quadrangle of Kinzel Spring, Blount County. Two of these rock cuts, the numbers 1 and 3, were selected to be analyzed by a computer program using the energy-based approach. Pictures of these rock slopes are depicted in Appendix A.

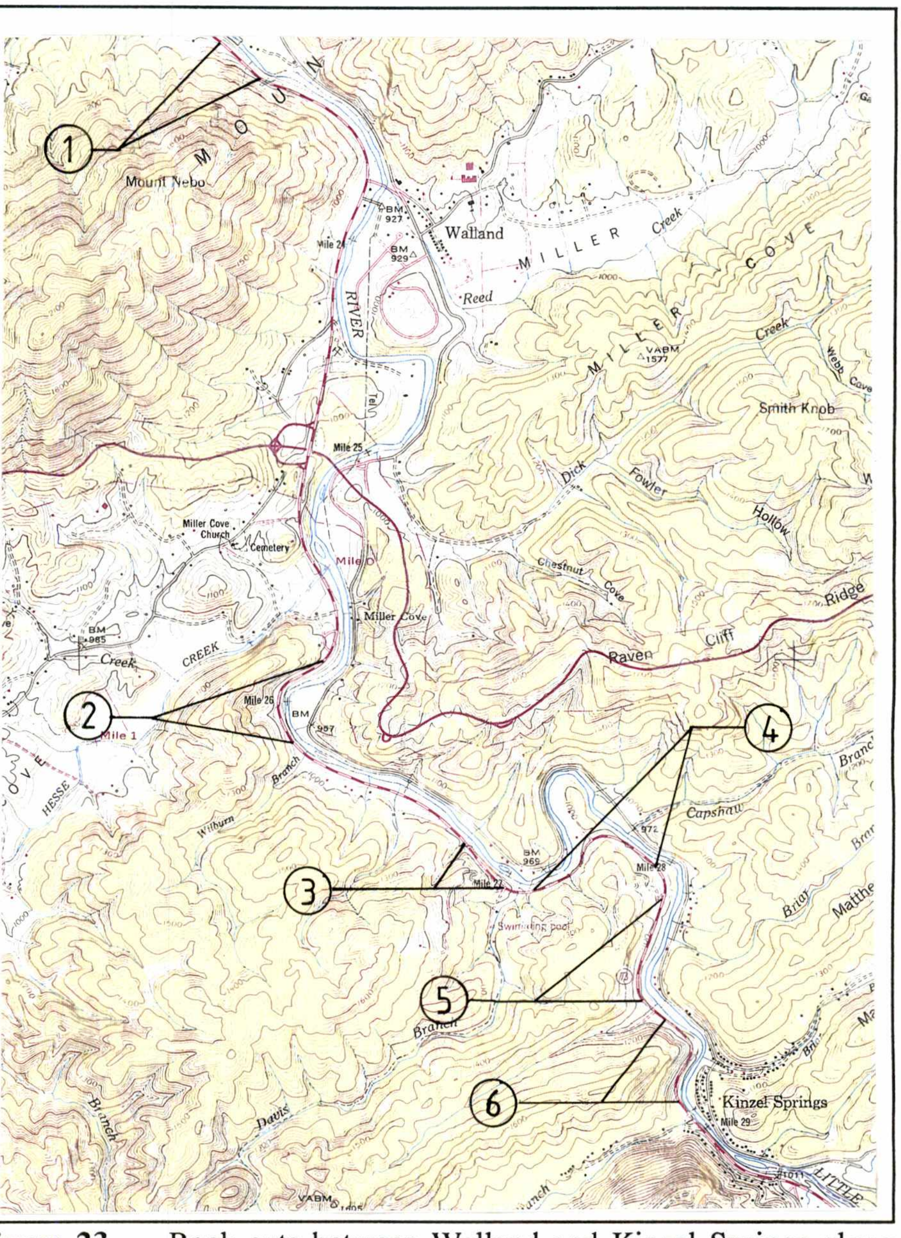

Figure 23 Rock cuts between Walland and Kinzel Springs along Highway 73, Blount County (Quadrangle of Kinzel Springs, Tenn., 1978).

4.2.2 Rock Units

For this study rock cuts 1 and 3 were chosen as the places to apply the new slope stability model because of the conditions of instability that the folded rock displays on these sections (see Fig. A-1 and A-3 in Appendix A). An explanation and distribution of the geological groups of these rock cuts are presented on the Geologic Map of Tennessee made by Hardeman et al., 1966 (see Fig. 24).

The geological formation of rock cut 1 on Chilhowee Mountain located before the entrance of Walland is considered part of the Sevier Shale - Osv (Middle Ordovician). This was assumed because of two important facts: the weathering conditions of the rock and the location of the rock cut on Figure 24. The Sevier Shale consists of shales and sandstones of Middle Ordovician (formed 600 million to 300 million years ago) combined with thin to thick beds of several other lithologies. The latter is a condition quite defined along of the rock cut as well as the high folding of the rock. The high degree of folding was due to the action of the Great Smoky fault which put the Middle Ordovician shale below it in contact with formations of the Chilhowee group on the southeast face of Chilhowee mountain (King et al., 1968). Actually, a great part of the section southeastward of the original rock cut is covered by a tall retaining wall of concrete constructed because of falling rocks from the top of the slope.

The geological formation of rock cut 3 located southeast of the village of Miller Cove is considered part of the Walden Creek group - pCw (Ocoee series from the later Precambrian). Describing this site is more difficult because this group is fórmed by four mixed formations known as: Licklog, Shields, Wilhite, and Sandsuck. The causes of this

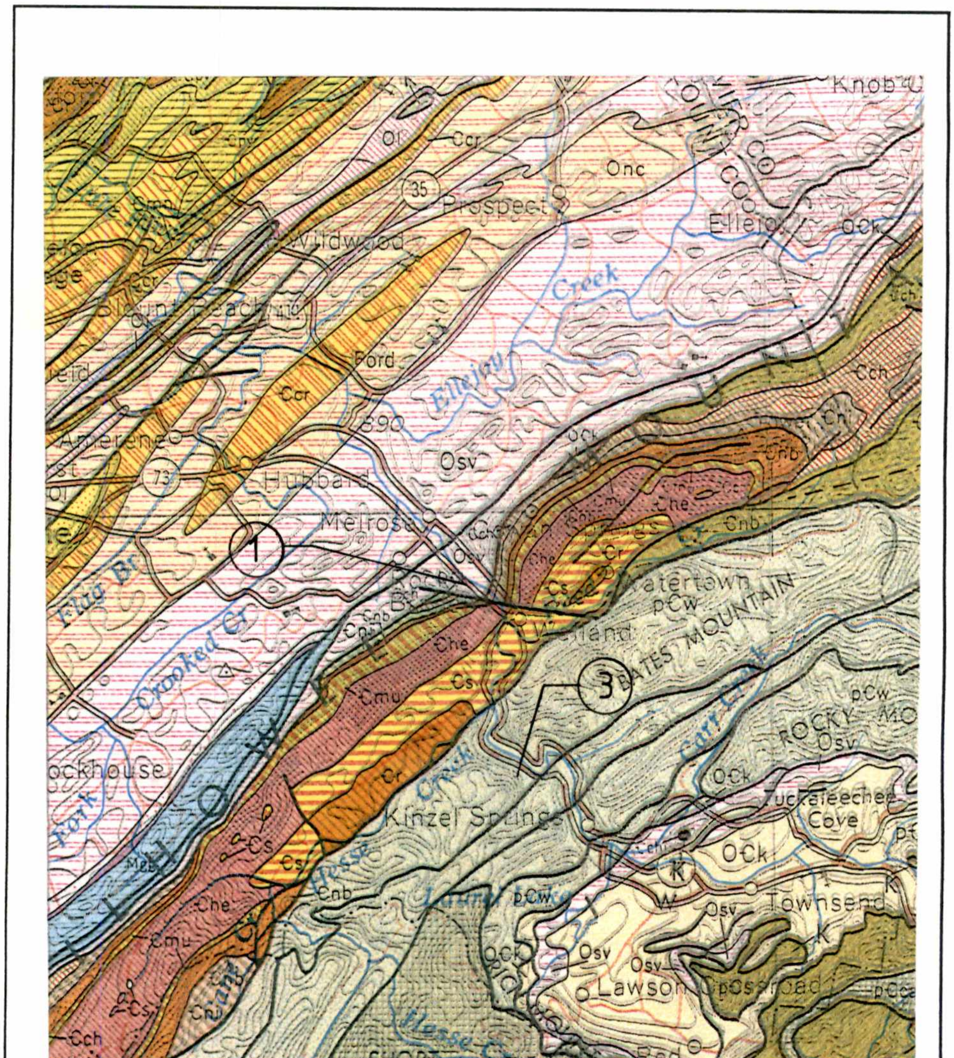

Figure 24 Rock formations of the rock cuts 1 and 3 (Hardeman et al., 1966).

disorder are the weakness of the shales and siltstones, common to the formations, and the fact that the group is underlain at shallow depth by the Great Smoky fault (King et al., 1968). In particular, the site is dominantly composed of weathered shale at the top and of siltstone at the bottom of the rock cut as it was observed on the field. These characteristics are more similar to those of the two last formations of the Walden Creek group, the Wilhite and Sandsuck formations.

4.2.3 Lithology

With respect to the site conditions the following is a description of each rock cut based on the rock units mentioned in the foregoing section.

The Sevier Shale located in rock cut 1 is in general defined as follows:

(a) calcareous, bluish-gray shale, weathers yellowish-brown; with thin gray limestone, sandstone, and siltstone layers.

The whole section of rock cut 1 shows the typical yellowish-brown color mentioned above indicating the high level of weathering that is affecting the rock. This color is more intense close to the spring located in the middle of the rock cut. The rock is also more brittle and weak, and it almost becomes similar to a big mass of red-brown soil going southeast of the rock cut. This can easily be understood because the natural slope of the mountain tends southeastward. The rock formation is also highly folded displaying parallel laminations of very thin layers showing no spacing among the surfaces. Rodgers (1953) described these thin layers as mainly formed of shaly limestone and red limy quartz sandstone. Shaly limestone when weathered breaks down into yellow shaly chips. With respect to the limy quartz sandstone it weathers into a deep sandy or loamy soil with porous chips and blocks of brown ferruginous sandstone from which all lime has been leached. Furthermore, it is possible to see slickensides on the big chunks of fallen rocks indicating the high degree of deformation of the rocks in the past years.

As the Walden Creek group contains four different formations the description at this point will be limited to the last two members, the Sandsuck and Wilhite formations. This assumption is based on the field conditions observed on the site of rock cut 3.

The definition of the Sandsuck and Wilhite Formations are, respectively:

(a) olive-green and gray, argillaceous, micaceous shale with coarse feldspathic sandstone and quartz- pebble conglomerate.

(b) gray to green siltstone and slate with interbeds of pebble conglomerate and sandstone, and quartzite.

Throughout the rock cut 3, it is easy to see how the rock has been complexly folded and metamorphosed at different degrees of weathering. The rock of the cut at the level of the highway is still hard but very brittle, of uniform texture, and composed of fine-grained particles. The color ranges from dark-blue to gray and, due to intensive weathering, to clear green. This rock can be considered as being formed of siltstone and sandstone. A feature characteristic of this rock type is its grittiness. There are in the middle of the rock cut massive formations showing some folding conditions and a rough surface composed of medium to coarse grains with a shaly or sandy aspect. Ascending the wall it is possible to see interbedded layers and lenses of sandstone and shale, totally weathered, of clear color ending at the top with a material that looks like argillaceous shale. The rocks on the slope, at both sides of the highway, display a northeastward-dipping cleavage. The thickness of the bedding planes ranges from less than 12.5 mm up to 600 mm, approximately.

4.2.4 Permeability, Moisture, and Weathering

These particular parameters are highly related to each other because of the actual conditions that the rock mass shows on each of the rock cuts of the study area.

For rock cuts 1 and 3, no testing method was used to evaluate the permeability, but there is clear evidence of water contact or seepage through the joint sets and bedding, which permits one to assume that the rocks have a high degree of saturation and high permeability.

In rock cut 1 the saturation of the rock mass is particularly evident because of the presence of several springs on the upper part of the slope cut indicating that the water table is near the surface. Most of the rock cut displays seepage throughout the highly folded and brittle bedding allowing the assumption of a high degree of permeability. Owing to the latter features together with the presence of water, the rock formation of this site (Sevier Shale) can be described as very intensely weathered to decomposed.

With respect to the rock formation in rock cut 3 (Walden Creek Group), there are many different conditions. As in rock cut 1, the rock mass in this section is highly folded and brittle, but these features were observable after the excavation of the cut. The rock mass is totally decomposed from top up to a depth of approximately 2.5 to 3 meters. Below this level the condition of the rock mass can be described as moderately weathered throughout the cut. It seems that chemical weathering is not affecting the rock mass, even though at the center of the section there is some sort of discoloration or oxidation on the rock. In addition, it is possible to see on the east side of the cut a thin layer of water contact coming out from the joint sets which keeps the rock damp. The soil at the border of the highway is also saturated. On the west side of the cut, the bedding planes do not show presence of water contact and the cut seems to be dry.

4.2.5 Hardness and Strength

Two tests were conducted on the rocks of the two sites under study. One test was to measure the hardness by scratching the surface of a rock specimen with a knife. The second test was conducted using the Schmidt hammer. The Schmidt hardness has been approximately correlated with the compressive strength.

The Sevier Shale in rock cut 1 proved to be very weak and fissile when the hand specimen was scratched with a knife exerting light pressure. This shale was, therefore, considered to be soft to very soft. Due to the variability of the rock in the Wilhite formation, beds or lenses of other types of rock, i.e. sandstone, conglomerate, or slate, in rock cut 3, this rock material displayed a range from moderately hard to moderately soft when the hand specimens were scratched with a knife.

To measure the strength of the rocks, 100 readings along rock cut 1 and 204 readings along rock cut 3 were taken with the Schmidt hammer. Because of the high number of Schmit hammer readings equal to zero in rock cut 1, an average of 4.5 was obtained for the Sevier Shale. This corresponds to a compressive strength value of less than 10.0 kN/m^3. For the Wilhite formation of the Walden Creek Group in rock cut 3, the average of 11.5 using the Schmidt hammer test yielded a compressive strength of approximately 15.0 kN/m^3. Both magnitudes were obtained using a graph that correlates the compressive strength with the Schmidt hardeness (Hoek and Bray, 1981).

4.3 **Discontinuities**

Discontinuities are the major factor in the evaluation of rock masses for its influence in engineering properties, and the stability of man-made slope cuts into the rock mass.

The features of the rock mass, such as weakness and brittleness in rock cuts 1 and 3, have been defined by the faulting and folding that the area suffered in the past as it was previously explained in the section 4.1. In the following paragraphs, some observable physical characteristics such as orientation, spacing, openness, and surface conditions are used to describe the joint sets and bedding planes forming the rock mass of both sites. Two more features are added separately to describe physical aspects of the study sites. These are the fold axes and the cleavage located in the folds.

4.3.1 **Bedding**

Rock cut 1 is approximately 200 meters long and has an orientation that strikes N 70° W with a dip of 90° NE. This slope cut to the east is limited by a concrete retaining wall. The slope cut shows a folded and brittle rock bedding. Independent of the latter conditions, the limbs and hinges of the folds are perfectly defined, only a few of the hinges are overfolded. Figure 25 depicts, according to the contour of the pole distribution, the mean strikes of the limbs formed by the bedding planes. From this plot the mean orientations are northwest bedding: strike S 80° W, dip 72° NW; southeast bedding: strike N 4° W, dip 55° NE. The mean orientation for the intersection line of these beddings is: trend 57° NE, plunge 50°. It is still possible to see boreholes on the slope, but due to the actual conditions of the rock there is no evidence that excessive charge split the rock during excavation. In general, the rock bedding contains thin to thick beds of different lithologies ranging in thickness from 2 to more than 50 mm. In this section, all rock surfaces of the bedding planes are highly weathered but they can be defined as slightly rough and planar. Also the surfaces of this rock formation depict a sort of parallel striations that is believed to be slickenside. The latter characteristic is possible depending on the degree of deformation that the beds suffered in the past giving origin to zones of weakness into the rock mass. On the east side of the slope the rock mass is totally decomposed between the water stream and the concrete retaining wall. Furthermore, this part of the section is the most highly faulted compared with the rest of the slope cut. At this particular location, the bedding planes are dipping between 27 and 45 degrees.

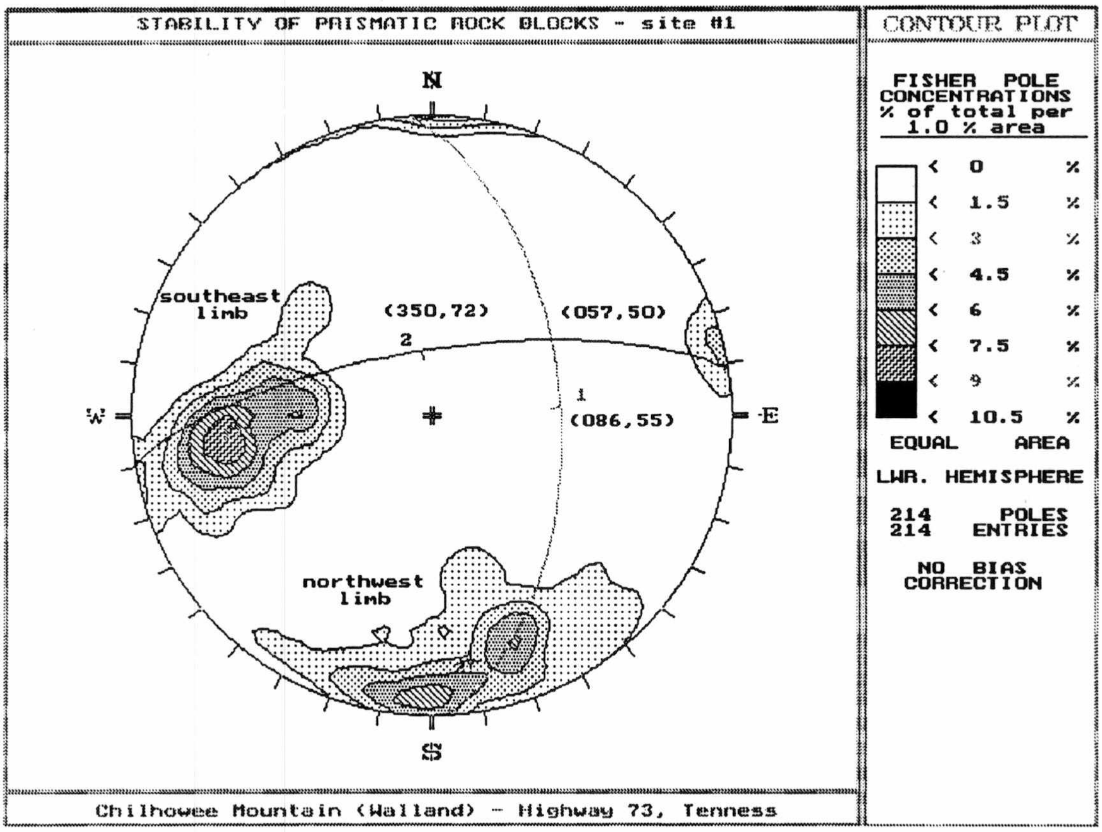

Figure 25 Mean strikes of the bedding planes of rock cut 1 in Chilhowee Mountain at Walland, Highway 73.

With respect to rock cut 3, the length is approximately 300 meters. The strike of the rock cut is in average N 35° W with a dip of 80° NE. The rock bedding of this formation can be described as folded and brittle but less intensively weathered than that of the rock cut 1 at the level of the highway until approximately 2.5 or 3 meters below the top of the slope cut. Above this boundary the bedding planes mainly formed of shale are totally decomposed. The bedding planes located east and at the center of the slope cut are dipping between 25 and 45 degrees, and on the west side of the section they are dipping from 55 to 75 degrees. From one end of the slope cut to the other, not all of the folds are continuous. Many of the limbs and hinges are sheared due to the extensive faulting along the section. In addition, several of the hinges are also overfolded. The bedding planes are mostly formed of beds of siltstone and sandstone with lenses of shale and limestone. The thickness of the beds ranges from less than 12.5 up to 300 mm thick. In general, all rock surfaces are moderately weathered, and they can be assumed as moderately rough and planar. Figure 26 shows the orientations of the bedding planes and the two main set of joints. The mean strike of the bedding planes according to the contour of the pole distribution is as follows: N 47° E, dip 42° SE.

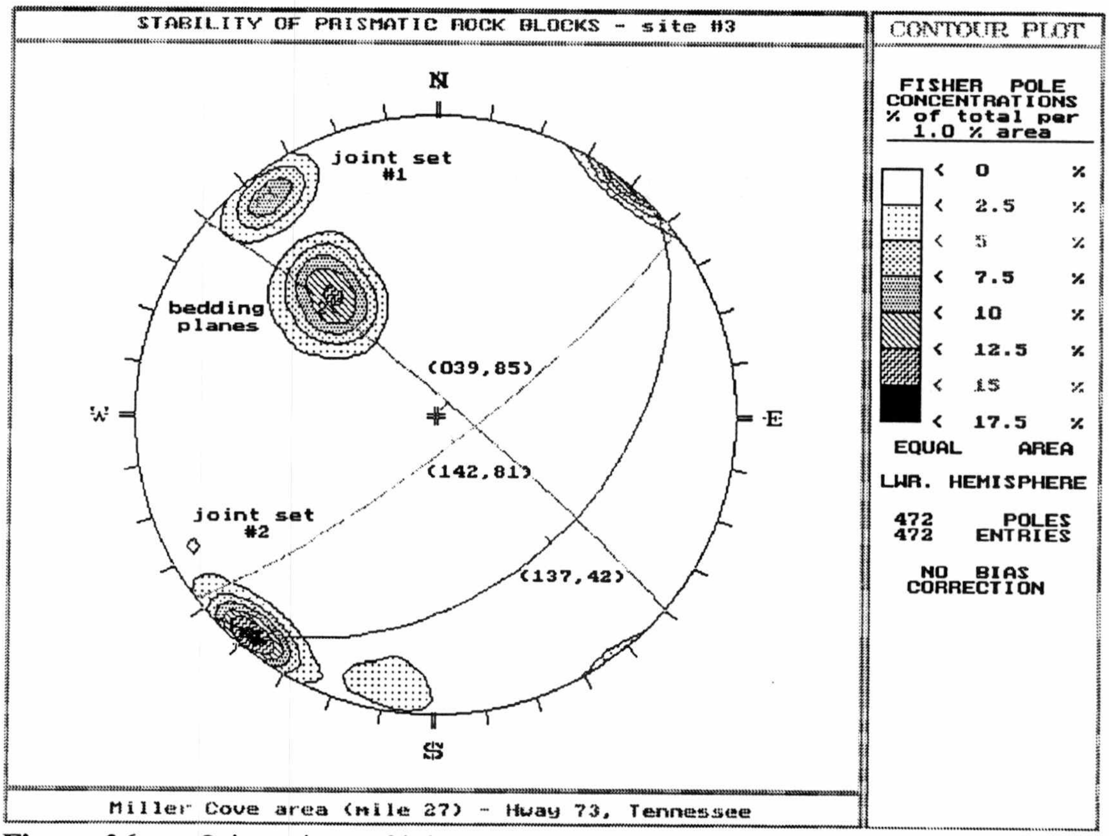

Figure 26 Orientations of joint sets and bedding planes of rock cut 3 in the area of Miller Cove, Highway 73.

4.3.2 **Joints**

Joints are fractures in rock that have originated in response to an applied stress. These fractures may have different orientations within the same structures, depending on their modes of origin. As for the shale material of rock cut 1, there is some jointing between the interbedded layers or bedding planes of the folded rock. The bedding joints are filled with weathered material from the same rock formation, even though there are a lot of small veins scattered at random on the limb surfaces filled with what seems to be quartzite. The thickness of the filling between the bedding planes varies from 1 to 12.5 mm. These bedding joints are mostly truncated east because of the weathering conditions of the rock and due to the presence of several small faults along the slope cut. The orientation of the bedding joints is assumed to be the same as that of the bedding planes (see Figure 25). The aperture or openness of these joints ranges from slightly open to open (1 to 16 mm). With respect to the spacing, the range is from very closely spaced to moderately spaced (less than 25 to 300 mm). This rock formation does not display defined joint sets except for those of the bedding joints. In addition, the small veins on the limb surfaces form planes of weakness making them responsible for the condition of brittleness of the rock.

In rock cut 3, two main joint sets are well defined. Figure 26 shows the normals to the major planes with an average plane for each discontinuity. These joint sets are at almost orthogonal angles to each other and are almost orthogonal to the bedding planes as seen in the stereonet projection. The orientation of these joint sets are as follows: joint set #1: N 52° E, dip 81° SE; joint set #2: N 51° W, dip 85° NE. East of the slope cut, the openness of these joint sets ranges from slightly open to moderately open (1 to 19 mm). These joint sets are mostly filled of decomposed material from top of the slope which was assumed to be of the Sandsuck formation. After the center and westward areas of the slope cut, the openness reaches up to a magnitude of approximately 150 mm or wider. The spacing of the joints is from very closely spaced to closely spaced (less than 25 to 100 mm) on the east side, and from moderately spaced to widely spaced (25 mm to 900 mm) on the west side of the rock cut. Filling of calcite or quartzite was not observed on the bedding surfaces along of the slope.

4.3.3 **Folds**

As was explained earlier the present arrangement of the rock formations of the study area is the result of the effects of the faulting and folding between the Valley and Ridge Province and the Unaka Mountains. Furthermore, the folds formed at different ages have been affected by metamorphism producing complex relations as seen in individual exposures along Highway 73 in Blount County, Tennessee.

Rock cut 1 displays an uncommon type of fold: cylindrical-shaped folds. These sort of folds can now be seen because of the slope cut that was made to build the new section of Highway 73 surrounding Chilhowee mountain. As was explained in previous sections, the rock formation is mainly thin-bedded calcareous, bluish-gray shale. Although the folds are of cylindrical shape, they are not continuous throughout the rock cut. It was mentioned before that eastward of the slope there is a faulted zone in which the folds are cut off and the rock formation is highly deteriorated. Most folds of the section trend northeast while their northwestward-dipping beds are much steeper (60 to 85 degrees) than the southeastward-dipping ones (28 to 55 degrees). In addition, the limbs of these folds are of unequal length. Thus they can be considered as asymmetric folds. In general, the folds in this exposure vary from open to close, indicating a moderate degree of deformation, and ranges in attitude from upright to inclined. Figure 27 shows the fold axis calculated using a mean plane through the contoured distribution of normal vectors to the folds in the rock cut 1. The fold axis evaluated in this way trends 26° NE and plunges 47°.

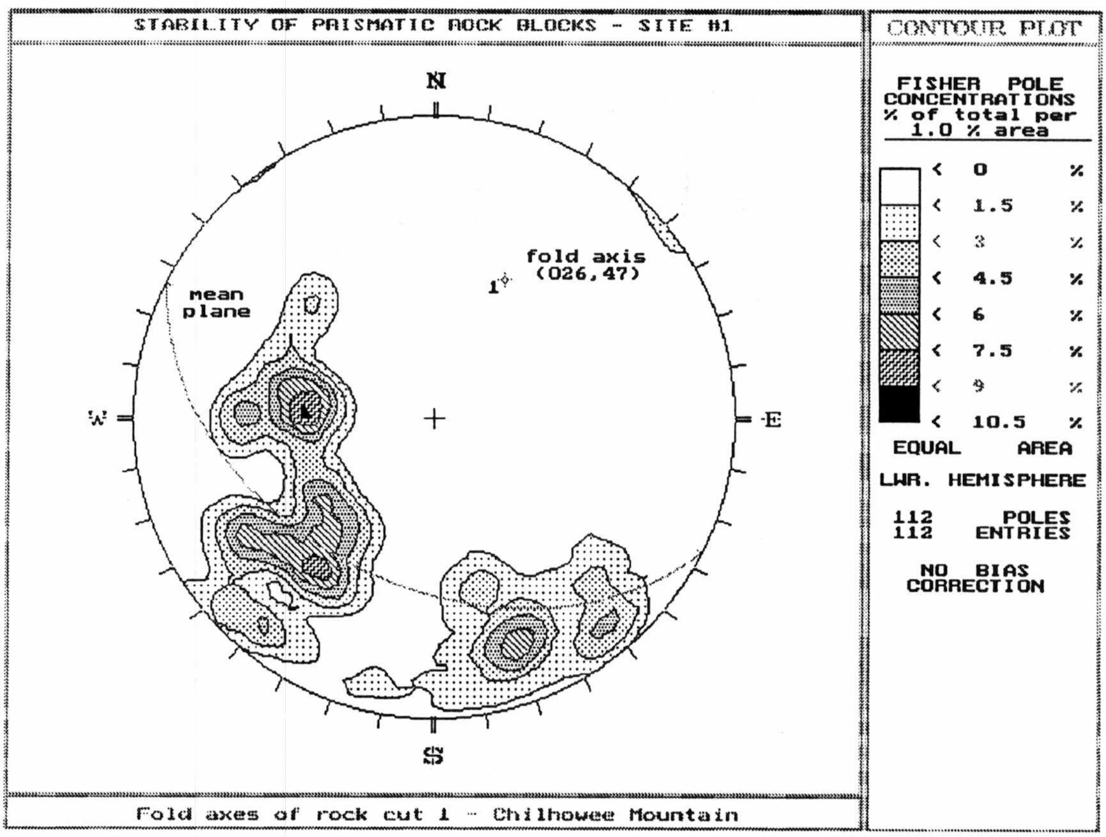

Figure 27 Contour of normal vectors to the folds in rock cut 1 located at Chilhowee Mountain, Walland.

In the exposure of the folded fine-grained strata of the Walden Creek Group in rock cut 3, the folds range from close to tight. Several of them are strongly overturned, indicating a higher degree of deformation when compared with that of rock cut 1. Furthermore, the shape of the folds varies from rounded to angular. The latter conditions can better be observed on the folds at the level of the highway. Above this level, approximately 2.5 to 3 meters, the bedding planes of the folds are crossed out by several southeast-dipping thrusts or local faults which reflects the northwestward movements of the major faults mentioned at the beginning of this section. As the shape of the folds is variable and depends on the thickness of the folded bedding, the fold profile of this rock formation was used here to verify in another way the amount of strain. The numerical ratio between the layer-thickness in the limb to the layer-thickness at the hinge gives a range from 0.05 to 0.30, so that, the thickening of the fold hinges and thinning of fold limbs probably indicates that flexural-flow mechanism of folding was at least involved in the deformation. In this section, the folds trend northeast with a range in attitude from upright to overfold. Figure 28 depicts the contoured distribution of normal vectors to the folds in the rock cut 3. The mean orientation of the fold axis calculated trends 43° NE and plunges 54°.

Pictures of both sites showing the geological characteristics previously mentioned can be seen in Appendix B.

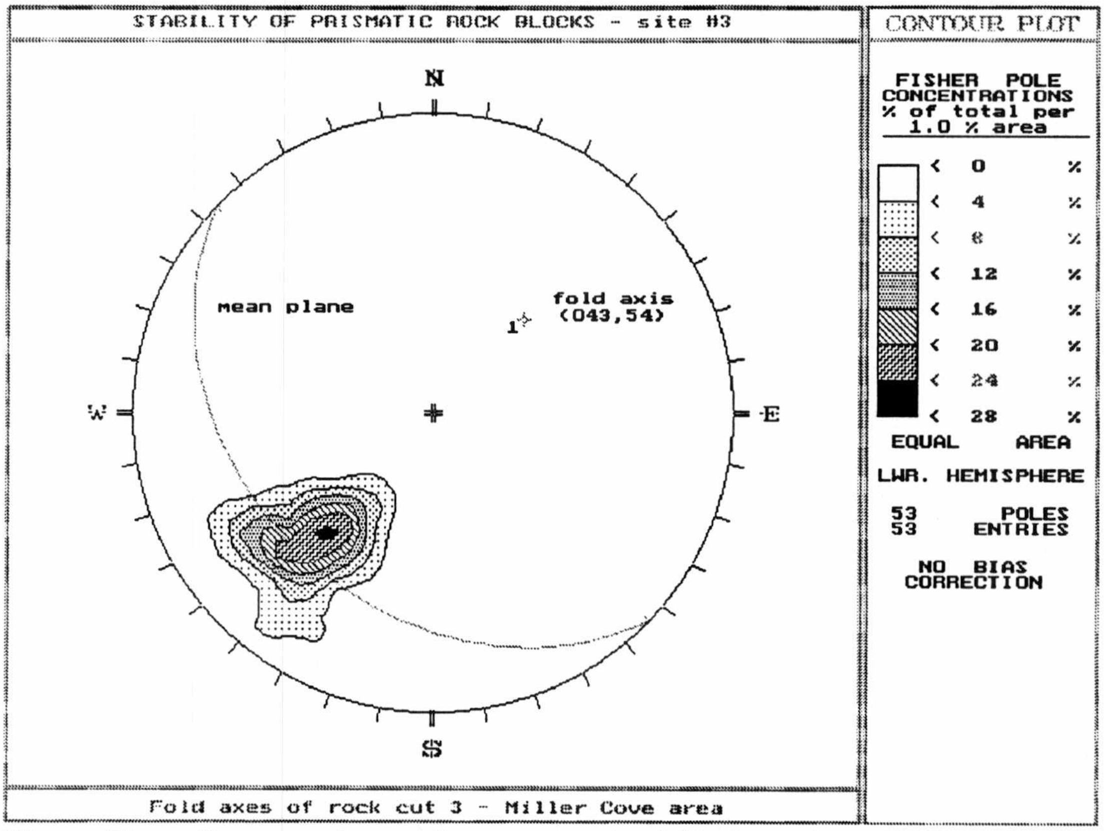

Figure 28 Contour of normal vectors to the folds in rock cut 3 located at the Miller Cove area.

4.3.4 **Cleavage**

The term *cleavage* is defined by Compton (1985) as "... a foliation due to rocks pitting readily into sheets, lens-shaped bodies, or linear bodies."

Cleavage was not observed on the fold hinges of rock cut 1. Two reasons that could explain the absence of this feature are the actual weathering conditions and the moderate degree of deformation of the rock. These two conditions do not mean that some sort of cleavage could not have existed on the folded rock in the past.

The presence of cleavage is more noticeable in rock cut 3. In this area, the cleavage can mainly be observed to the east and at both sides of the slope cut trending northeast, the same as the fold axes. The cleavage plunges steeply and ranges from 55 to 90 degrees. Owing to its physical characteristics, the cleavage of this rock cut is defined as axial-planar cleavage. This type of cleavage consists of parallel, closely-spaced fractures to the axial plane in the hinge areas of folds. The spacing of these fractures is in the order of approximately 2 to 5 mm, for the type of cleavage found in this area. Axial-planar cleavage is formed during folding of the bedding planes and is typical of the deformed, relatively strong and brittle rocks such as the sandstone and siltstone present in the area. Figure 29 shows the contoured distribution of cleavage poles located on the folds of rock cut 3. The great circle describes a mean orientation of the cleavage poles that trends 58° NE and plunges 75°. As was expected, the mean orientations of the fold axis and the axial-planar cleavage of rock cut 3 have a slight difference in magnitude but still keep the same northeastward trending.

4.4 Stability Analysis

Miller et al. (1977) have identified the zone along the foothills and mountains of the Unakas as one of the major areas with geologic hazards due to gravity movement in East Tennessee. In this area the combination of factors which includes steeply dipping beds, pervasive weathering, highly fractured rocks, steep and irregular terrain, and high annual rainfall result in high potential for various types of gravity movements, e.g. rockslides, rockfall, dip slope failure and flowage. The factors mentioned above have greatly affected the rock formations in the area of study mainly those previously identified as Ordovician (in rock cut 1) and Precambrian (in rock cut 3).

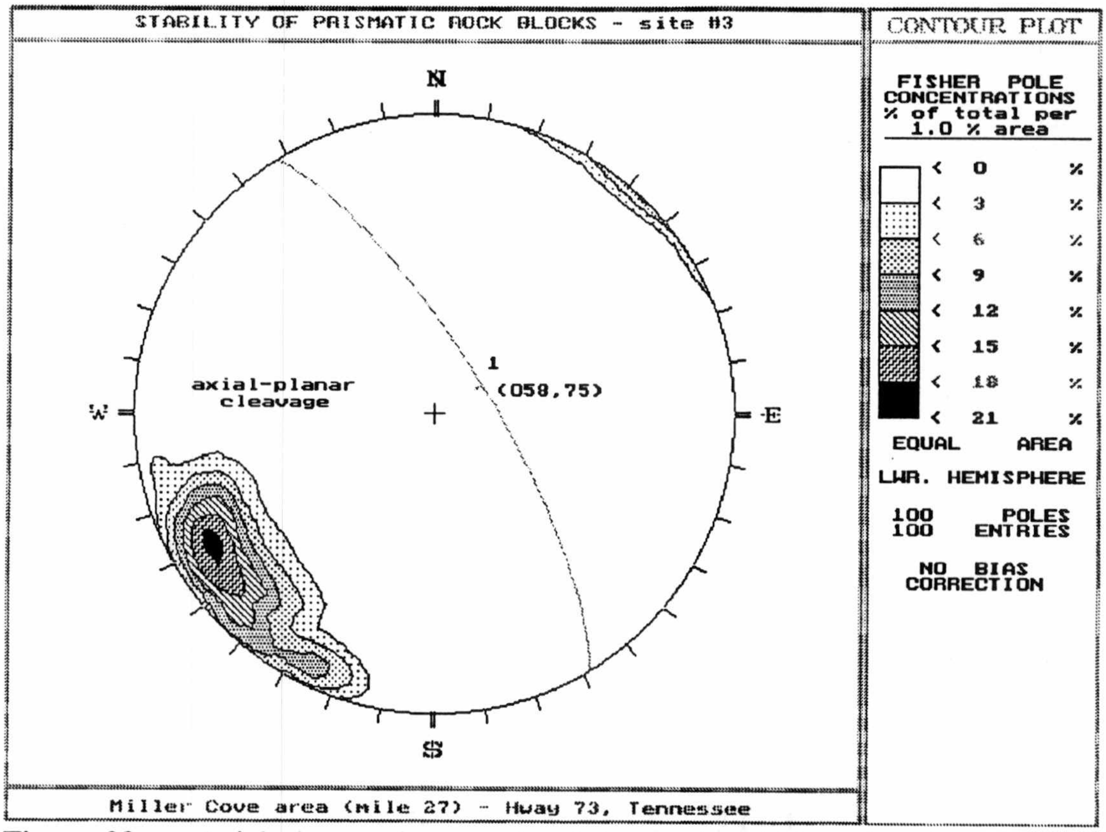

Figure 29 Axial-planar cleavage located on the folds of rock cut 3 at Miller Cove area.

As it was mentioned before, the goal of this study is to evaluate the sliding stability of two rock cuts along Highway 73 in Blount County, Tennessee, using the mathematical approach previously developed in Chapter 3. Field data necessary to apply the newly developed method includes measurements on the folds of rock cut 1 such as plunge and trend of the fold axes and plunge of the limbs. After the collection of the data, drawings are made of the true cross section, i.e. cross section perpendicular to the fold axis, to discretize the shape of the sections into failure planes.

4.4.1 **Analysis of Rock Cut 1**

In rock cut 1, the failure surface is related to the cylindrical folded rocks. Thus, two cylindrical-shaped folds of this cut identified as *fold a* and *fold b* were taken to discretize their shapes (see Figures 30 and 31). The following steps were taken in order to define the failure surface of both folds: first, a drawing of the true section of both folds is made to define the failure surface (see Figures 32 and 33); second, the discretization of the failure surface of each fold into planes is indicated by dots (see Figures 34 and 35); and third, the prismatic block of each fold is used to determine the length l_i and the angle θ_i, measured clockwise from the X direction, of each single plane. The parameters l_i and θ_i were defined in section 3.4 (see Figures 12, 36 and 37).

At this point it is important to remember again that the safety factor is dependent on block geometry, loading conditions, and friction angles. Since rock cut 1 is expected to be affected by seepage through the bedding joints and high weathering conditions, the friction angle for the Sevier Shale was assumed to be 27°. This value was taken from the book of Hoek and Bray (1981). The loading conditions were assumed due to gravity alone, and the geometry of each cylindrical fold was defined through the prismatic rock block. Thus, with the data obtained from the pictures and the prismatic blocks of both folds, the factor of safety for each cylindrical fold is evaluated using the computer program made specifically for this research study (see Appendix C). In addition, both folds were analyzed as wedge failures using the same failure surface of each fold (see Figures 38 and 39). In Table 2, a summary of the results can be seen for both the typical wedge failure (two-plane rock block) and the prismatic rock block. These results

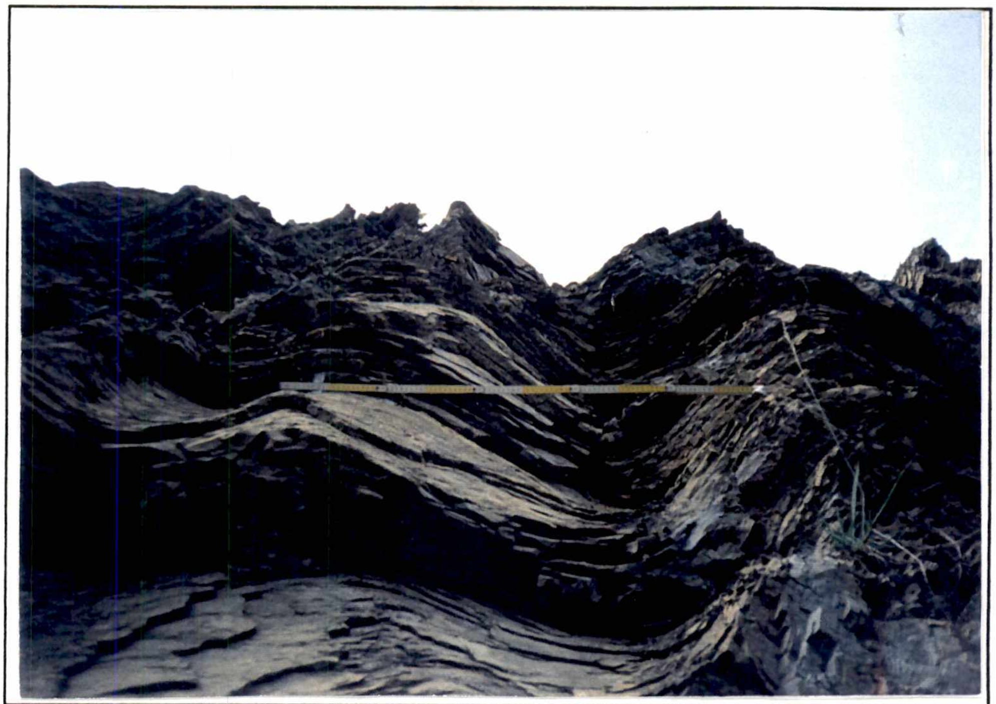

Figure 30 True cross section of fold *a* (scale of the meter is 100 cm).

Figure 31 True cross section of fold *b* (scale of the meter is 100 cm).

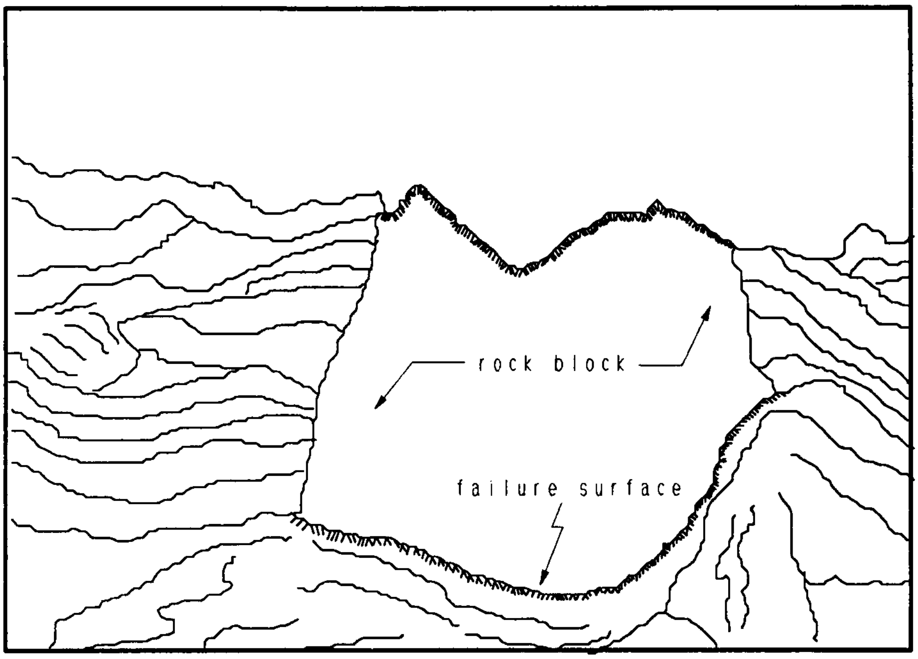

Figure 32 Idealization of the true cross section of fold a.

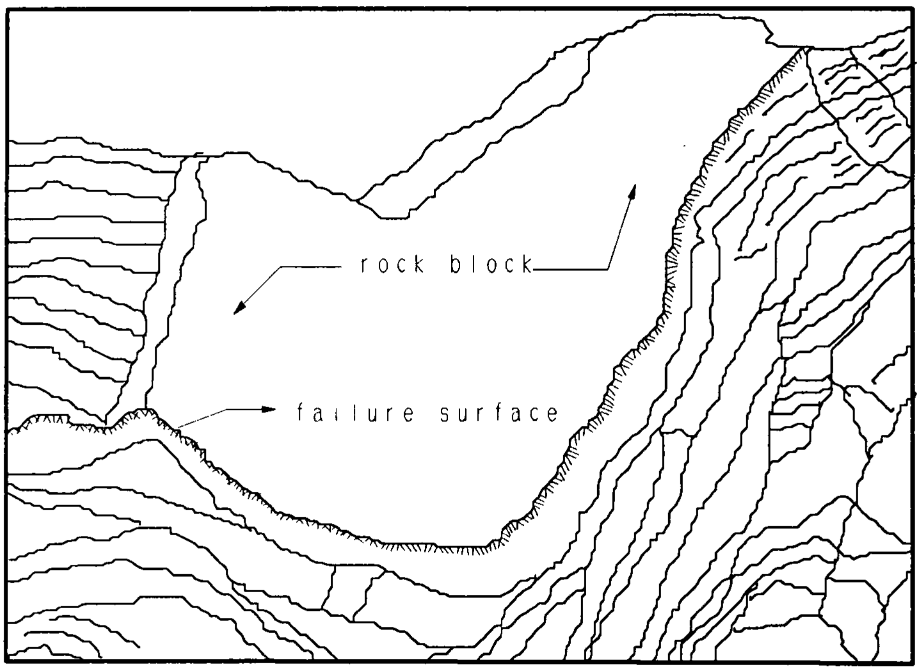

Figure 33 Idealization of the true cross section of fold b.

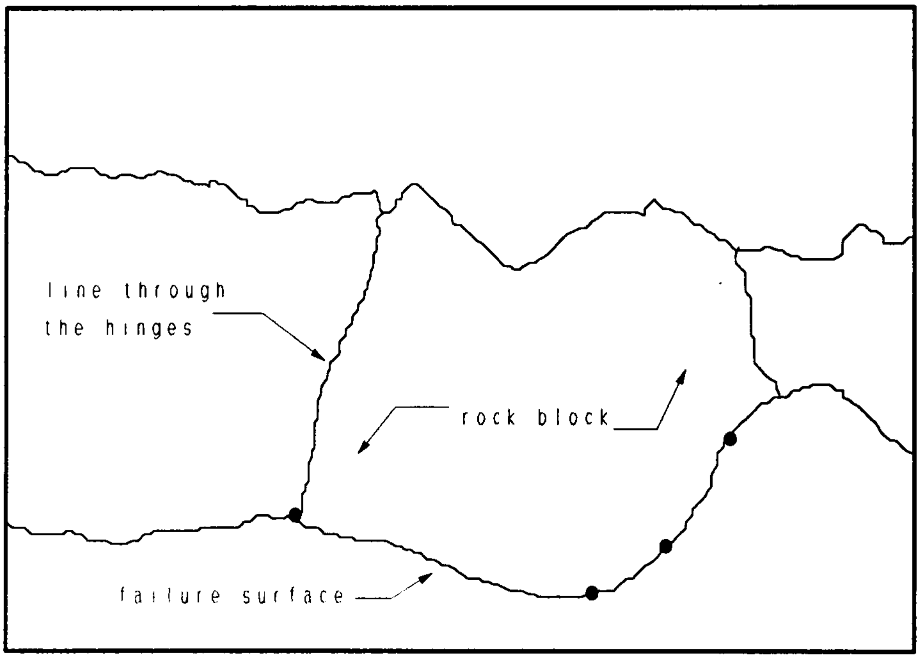

Figure 34 Discretization of the failure surface of fold a.

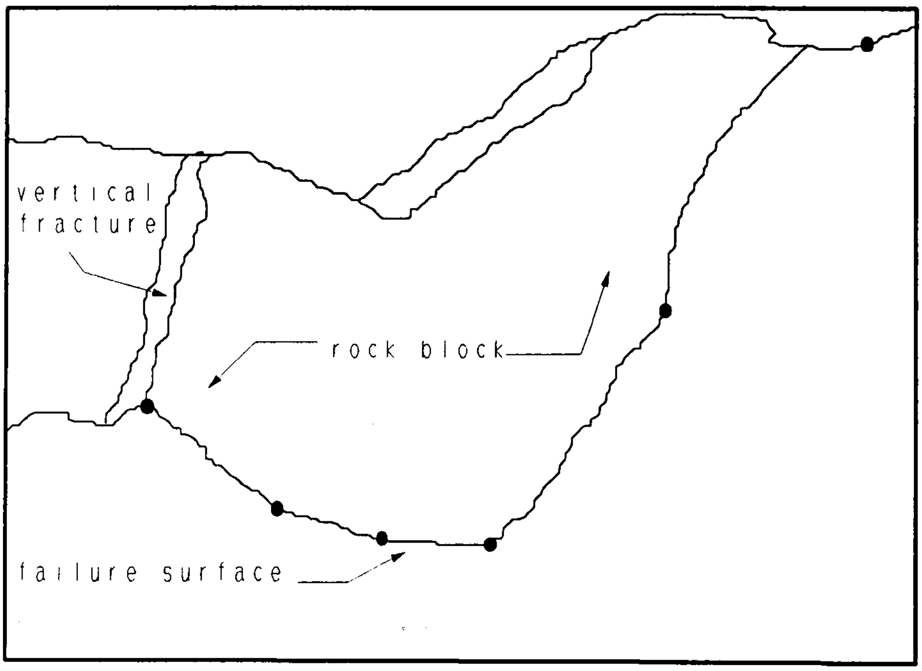

Figure 35 Discretization of the failure surface of fold b.

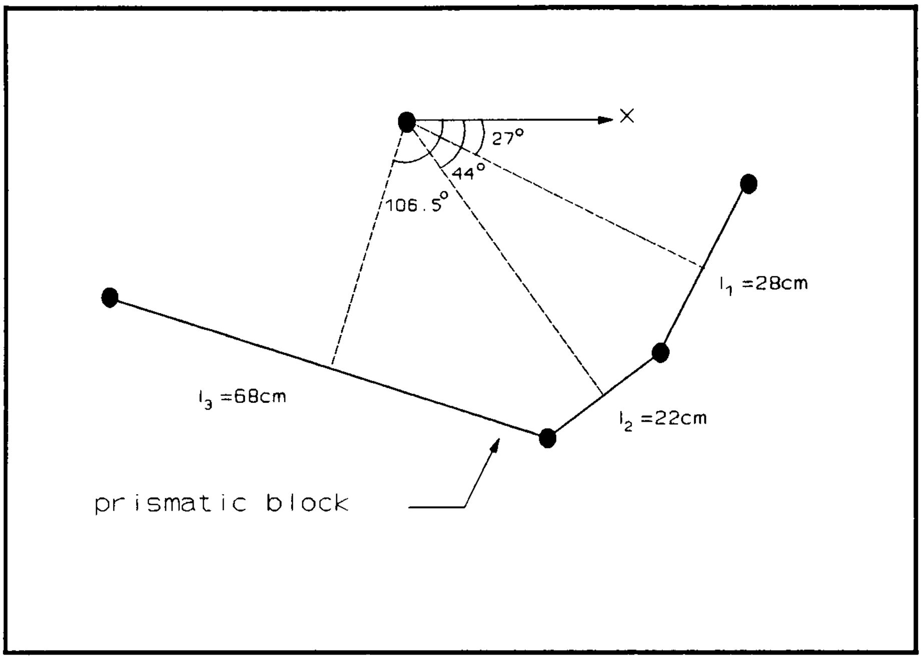

Figure 36 Prismatic block with three discontinuity planes defined by fold a.

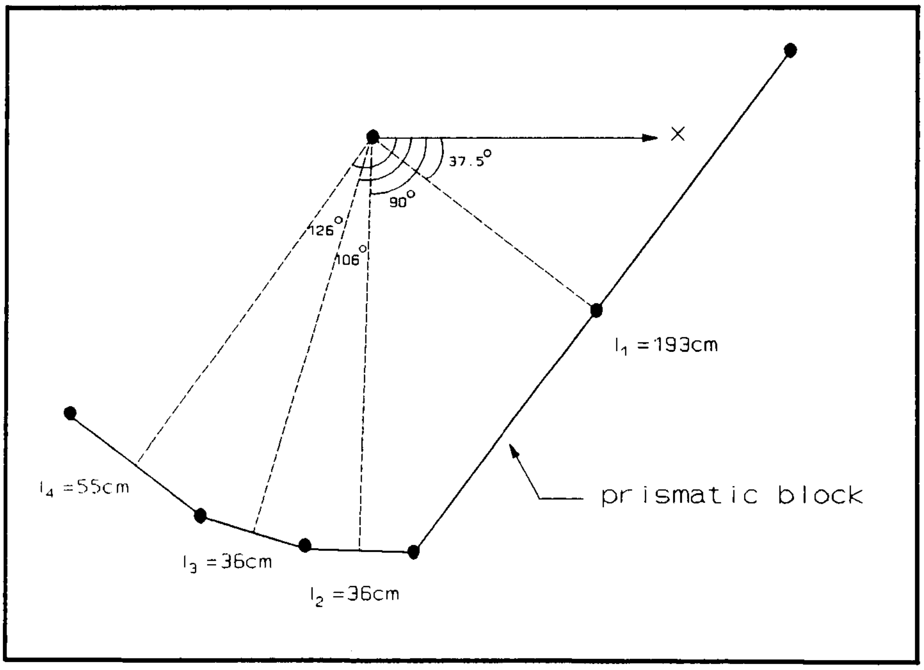

Figure 37 Prismatic block with four discontinuity planes defined by fold b.

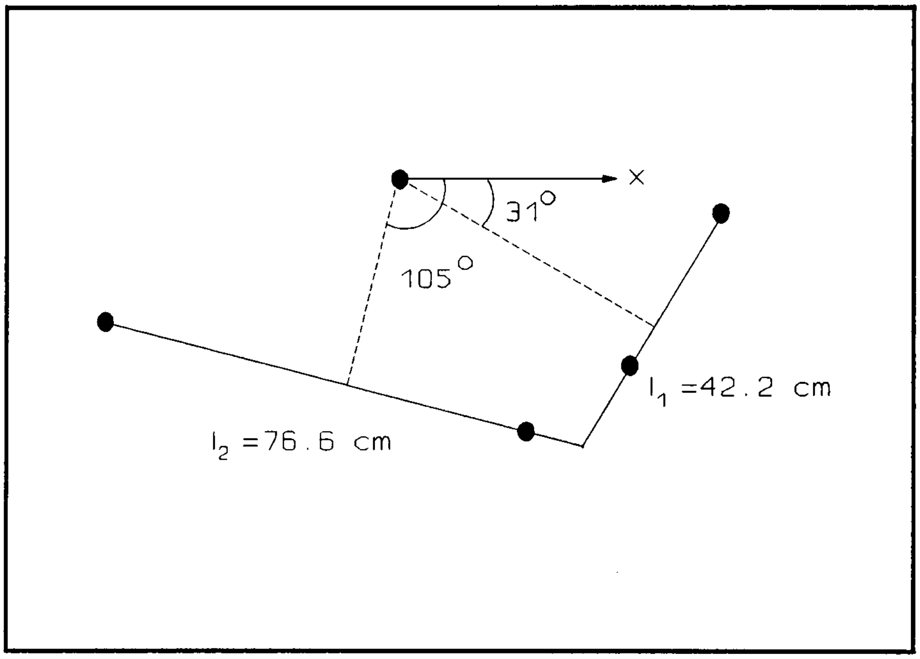

Figure 38 Analysis of *fold a* as a wedge failure.

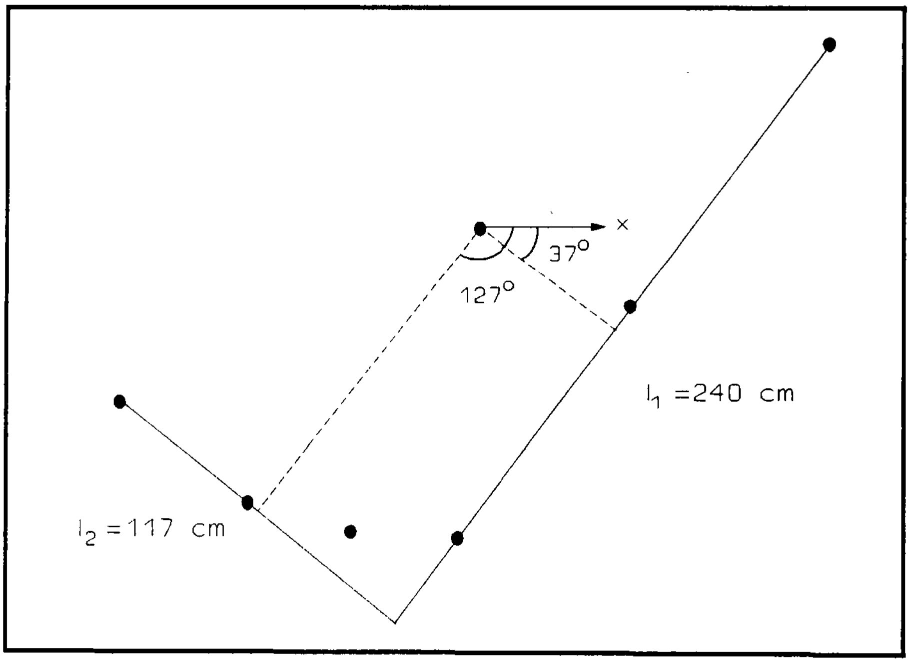

Figure 39 Analysis of *fold b* as a wedge failure.

Plane #	l_i (cm)	θ_i	ϕ	FS
Fold a				
fold axis: plunge = 37° ; trend = 60°				
case 1: wedge failure (Figure 38)				
1	42.2	31°	27°	0.785
2	76.6	105°	27°	
case 2: prismatic block (Figure 36)				
1	28.0	27°	27°	0.786
2	22.0	44°	27°	
3	68.0	106.5°	27°	
difference in percentage between case 1 and case 2 is: **0.0%**				
Fold b				
fold axis: plunge = 32°; trend = 32°				
case 1: wedge failure (Figure 39)				
1	240.0	37°	27°	1.14
2	117.0	127°	27°	
case 2: prismatic block (Figure 37)				
1	193.0	37.5°	27°	1.0
2	36.0	90°	27°	
3	36.0	106°	27°	
4	55.0	126°	27°	
difference in percentage between case 1 and case 2 is: **14.0%**				

Table 2 Summary of values of folds *a* and *b* for both wedge failure and prismatic block.

permit the establishment of a relationship between the number of planes contained in the prismatic block and the factor of safety for each cylindrical fold. For instance, fold *a*, with a plunge and trend of 37° and 60°, respectively, has a factor of safety as a wedge failure of 0.785, and for the prismatic rock block 0.786. For this fold there is no significant reduction of the safety factor because the failure surface discretized as a wedge failure practically fit the shape of the prismatic block with three discontinuity planes. The same analysis was done with respect to *fold b*. With a plunge and trend of 32° and 32°, respectively, the factor of safety for the wedge failure is 1.14, and for the prismatic block is 1.0. The reduction of the safety factor of this fold represents approximately 14.0% when the prismatic block is taken into account to define the four-plane block. In summary, these preliminary results of stability analysis of cylindrically-folded rocks suggest that the factor of safety may have a reduction in magnitude as the number of discontinuity planes contained in the prismatic rock block increases.

4.4.2 Analysis of Rock Cut 3

For rock cut 3, even though there are several folded rocks along this slope, the predominant kind of failure observed in the area is that of wedge failure. From Figure 26, it is possible to see three points of intersection defined by the two joint sets #1 and #2, and the bedding planes. These intersection points, the orientation of the rock cut, and the normals of the joint sets along with the bedding planes were plotted separately in Figure 40. In this figure, the bedding plane normals are indicated by the number 3 and the rock cut by the great circle. From this figure, it was determined that only the

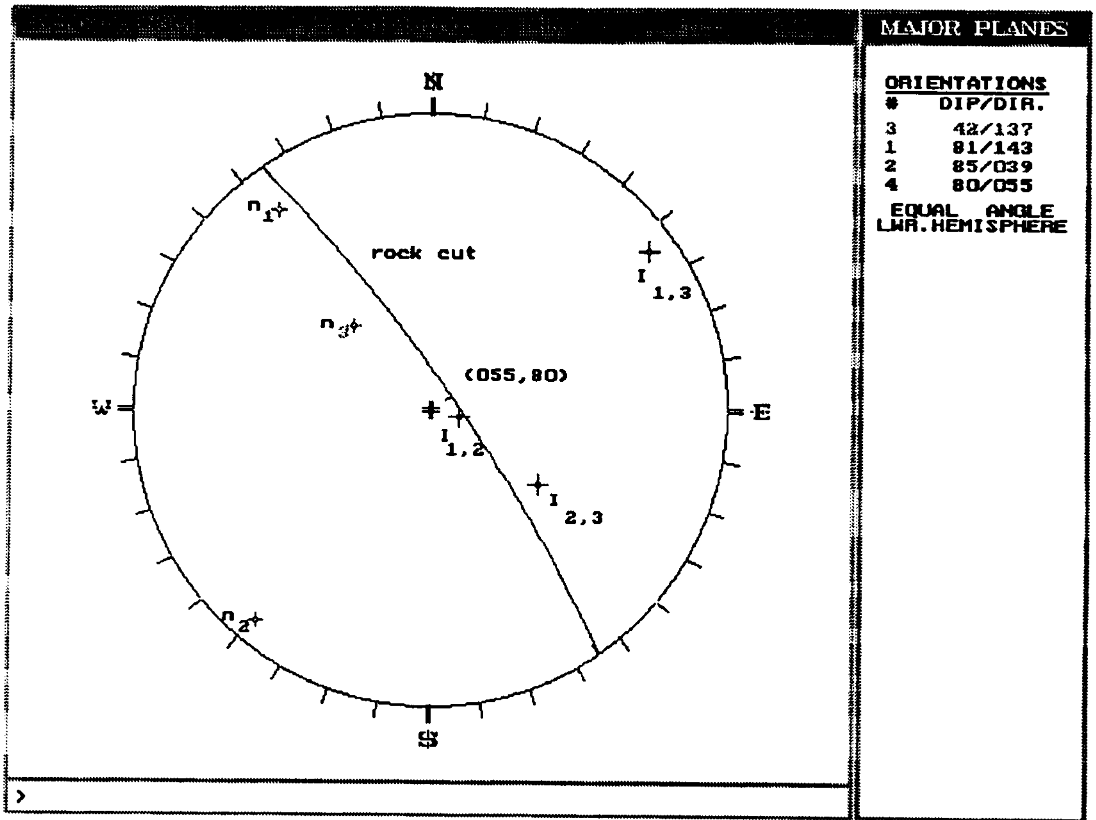

Figure 40 Graphical representation of the intersection points between the joint sets and the bedding planes of rock cut 3.

wedge formed by planes 2 and 3 could develop the necessary potential for sliding along the intersection line $\hat{I}_{23}$ (see Figure 40). Furthermore, the normals of planes 1 and 2 with respect to their location in the plot must be analyzed as a possible toppling failure. The latter condition was not considered as part of this research study. A friction angle of 30° taken from Hoek and Bray (1981) was assumed for the dampened siltstone and sandstone of rock cut 3. The safety factor with respect to sliding stability for the intersection between planes 2 and 3 is 0.75 (as determined by the new energy-based approach). This low value of 0.75 for planes 2 and 3 indicates a high degree of instability. A possible explanation for the inherent stability of this cut is that there is no freedom for the different rock blocks to move along the weak surfaces because other rock ledges of intact rock may be restraining such movements.

In summary, the sliding stability of rock formations is highly influenced by the physical characteristics of the rock mass, and the external forces that continuously shape and mold the earth's crust. This quantitative analysis of the deteriorated conditions in both rock cuts using the new mathematical approach with respect to the minimum potential energy stored in a prismatic rock block agrees and is supported by the qualitative evaluation of geologic hazards in East Tennessee performed by Miller et al. (1977), mentioned at the beginning of this section.

CHAPTER 5

CONCLUSIONS

The traditional methods of analysis for plane and wedge failures are based on limiting equilibrium analysis of statically determinate systems. In folded rocks, the potential failure (sliding) surface does not fit a simple wedge or plane model, and is better described as the limit $n \to \infty$ of a prismatic block with n contact planes. If the number of contact planes (n) is three or more, the distribution of normal forces among these planes is statically indeterminate. An explanation of the lack of methods is that the system of equations formed is statically indeterminate when more than two planes of discontinuity are simultaneously taken into account. The main goal of this research study was the development of a method to determine the stability, or more specifically, the factor of safety against sliding, for prismatic blocks with $n \geq 3$.

The solution for a prismatic block with three or more planes of discontinuity in contact with the rock mass presents two main problems: how to find the magnitude of the normal force acting on each plane and how to verify that the lines of intersection formed by the intersection of the discontinuity planes are all parallel. As was explained in Chapter 3, the distribution of normal forces was solved assuming an elastic and conservative system that minimizes the potential energy of the system. To verify that the lines of intersection are all parallel, the dips and dip directions of the planes were used to get the components of the unit vector perpendicular to each plane. Thus, the cross product between the unit vectors taken every two planes, permits the determination of the likelihood of a possible sliding of the rock block along these lines of intersection. Once these problems were solved and a computer program was developed, the second goal of this research was prompted by sliding stability investigations of two road cuts with cylindrically-folded rocks in East Tennessee.

In East Tennessee between Walland and Kinzel Springs, Blount County, along Highway 73, the area is considered of high geologic hazard due to the huge deterioration that the rock formations of different ages display. Conditions of instability such as rockslides, rockfalls, and dip slope failure are typical of this area. With this in mind, readings of strikes and dips on folded rocks were taken in two rock cuts designated as rock cut 1 and rock cut 3. Also, an identification of more possible areas of research in the near future were established in Chapter 4. The analysis of these folded rocks is initiated with the characterization of the folds. This was done through the discretization of the failure surface identifying the possible planes contained in a prismatic block with respect to the fold. This permitted the recognition of more planes around the fold than the two planes of a wedge failure typically used to calculate the factor of safety. The initial results from this analysis using the mathematical approach and comparing them with the typical solution of a wedge failure suggest that a significant reduction in the factor of safety when three or more planes of discontinuity are taken into account to form the prismatic block is possible. In addition, the upper and lower bounds of the prismatic block were determined to correspond with the wedge and plane failures, respectively. This new mathematical approach is a useful tool to determine the distribution of normal forces of prismatic rock blocks when they are sliding parallel to the line of intersection.

The model needs to be tested with more real prismatic block cases to determine if the factor of safety against sliding of prismatic blocks reduces in magnitude when the number of discontinuity planes increases.

In summary, the following points describe the goals reached in this research study:

(a) A new mathematical approach regarding the concept of minimum potential energy was developed to be applied in studies of stability analysis of prismatic rock blocks.

(b) To put in practice this new mathematical approach, a computer program was developed taking into account relevant aspects affecting the stability of prismatic rock blocks such as block geometry, loading conditions, and friction angles.

(c) The use of this mathematical approach through the computer program permits the analysis of the stability of prismatic rock blocks against sliding by determining a factor of safety when the discontinuity planes are acted on by friction forces.

(d) A reduction of the factor of safety might be possible when three or more planes of discontinuity are taken into account to form the prismatic rock block with respect to folded rocks.

REFERENCES

REFERENCES

Bloss, F. D. An Introduction To The Methods of Optical Crystallography. Saunders College Publishing (1961).

Compton, Robert R. Geology in The Field. John Wiley & Sons, Inc., New York (1985).

Goodman, R. E. Introduction to Rock Mechanics. Wiley, New York, first edition (1980).

Goodman, R. E. Introduction to Rock Mechanics. Wiley, New York, second edition (1989).

Goodman, R. E., and Shi, Gen-hua. Block Theory and Its Application to Rock Engineering. Prentice-Hall, Inc., Englewood Cliff, New Jersey (1985).

Hardeman, W. D., Miller, R. A., and Swingle, G. D.. Geologic Map of Tennessee. Tennessee Dept. of Conservation, Div. of Geology (1966), scale 1 : 250,000.

Hendron, JR., A. J., Cording, E. J., and Aiyer, A. K. Analytical and Graphical Methods for The Analysis of Slopes in Rock Masses-NCG Technical Report No. 36, Department of Civil Engineering, University of Illinois (1971).

Hoek, Evert, and Bray, John. Rock Slope Engineering. The Institute of Mining and Metallurgy, London (1981).

John, K. W. Graphical Stability Analysis of Slopes in Jointed Rock-Proceedings of The American Society of Civil Engineers, vol. 94, No. SM2, pp. 497-526 (1968).

King, P.B., Newman, R.B., and Hadley, J.B. Geology of the Great Smoky Mountains National Park, Tennessee and North Carolina. U.S. Geological Survey, Professional Paper 587 (1968).

Londe, P. , Asce, F. , Vigier, G. , and Vormering R. Stability of Rock Slopes, A Three-Dimensional Study-Proceedings of The American Society of Civil Engineers, vol. 9, No. SM1, pp. 235- 262 (1969).

Londe, P., Asce, Vigier, G., and Vormeringer R. Stability of rock Slopes-Graphical Methods-Proceedings of The American Society of Civil Engineers, vol. 96, No. SM4, pp. 1411-1434 (1970).

Mauldon, Matthew. Rotational Modes in Jointed Rock; a Generalization of Block Theory. Department of Civil Engineering, University of California, Berkeley, California, Ph D dissertation (1992).

Miller, Robert A., and Sitterly, Preston D. Geologic Hazards Map of Tennessee. Tennessee Dept. of Conservation, Div. of Geology, Enviromental Geology Series No. 5 (1977).

National Atlas of the United States of America. Physiographic Divisions of the Souththern Appalachian Mountains. U. S. Geological Survey (1968).

Safford, James M. Geology of Tennessee. Tennessee General Assembly, Nashville, Tennessee (1869).

Tucker, Charlie A., Jr. The Geology of Miller Cove, Blount County, Tennessee. The University of Tennessee, Knoxville, Dep. of Geol. Sci. Master's Science (1951).

U. S. Tennessee Valley Authority, Knoxville, Tennessee. Kinzel Springs Quadrangle, Tennessee, Blount County. U. S. Gelogical Survey (1978), scale 1 : 24,000.

Warburton, P. M. Some Modern Developments in Block Theory for Rock Engineering- Comprehensive Rock Engineering, Principles, Practice & Projects, vol. 2, p. 293-299. Pergamon Press, Ltd, Great Britain (1993).

Wilson, Robert L. Guide To The Geology Along The Interstate Highways in Tennessee. Tennessee Division of Geology, Report of Investigations 39 (1981).

Wittke, W. Methods to Analyze The Stability of A Rock Slope With and Without Additional Loading, in German, Rock Mechanics and Engineering Geology,Springer-Verlag, Vienna, Suppl. II, p. 52 (1965).

APPENDICES

APPENDIX A

Views of The Six Rock Cuts Identified Between Walland and Kinzel Spring, Tennessee

Rock Cut 1

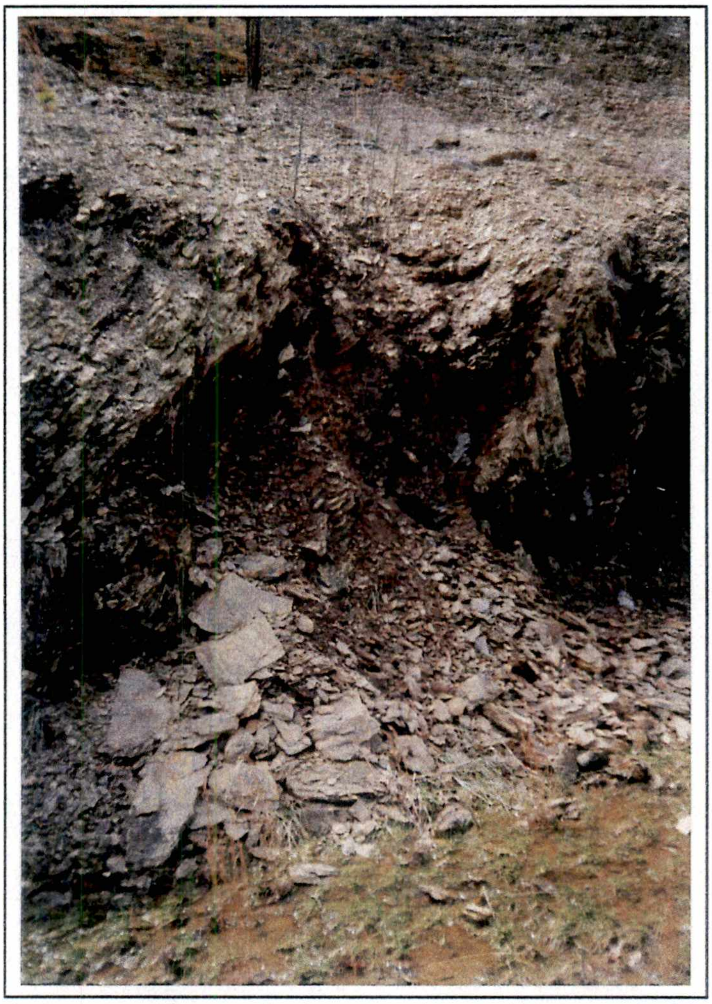

A-1.a View of the actual conditions of this rock formation.

A-1.b The presence of water is one of the factors responsible for the bad conditions of the rock.

A-1.c Because of the bad weathering conditions in the area a retaining wall was built east of the slope cut.

Rock Cut 2

A-2.a Lateral view of the slope rock.

A-2.b Bedding planes daylighting toward the highway.

Rock Cut 3

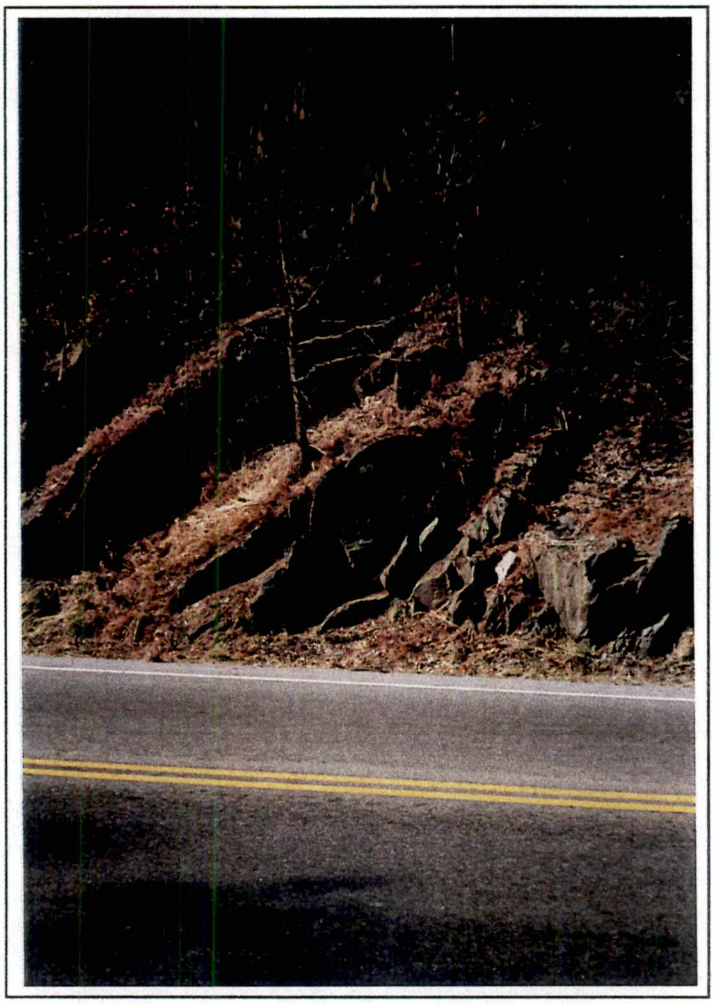

A-3.a View of the folded rock at the level of the highway.

A-3.b Arrow indicates top of the slope cut. The slope at top is highly weathered.

A-3c On the northwest side of the slope the bedding is steeply inclined.

Rock Cut 4

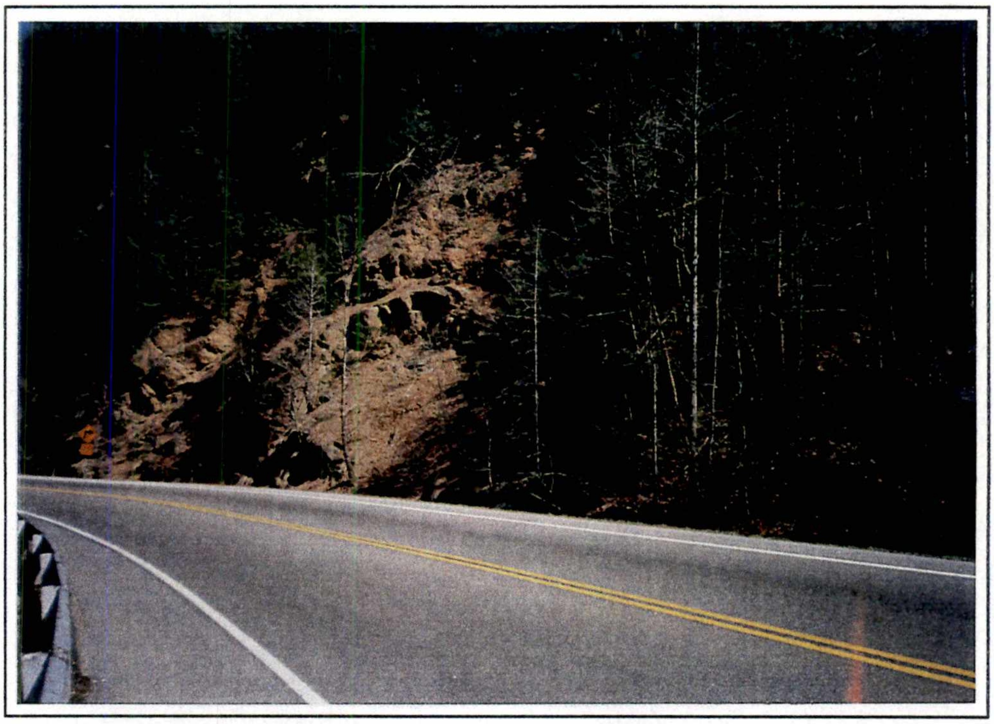

A-4.a Two conditions affecting the stability of this slope are the weathering and the brittle conditions of the rock.

A-4.b Another problem is the high plunge of the bedding.

Rock Cut 5

A-5.a General view of the slope showing a moderate degree of weathering.

A-5.b Shear zone located in the center of the bedding planes.

Rock Cut 6

A-6.a In this rock formation is possible to see that the planes of discontinuities are nearly vertical.

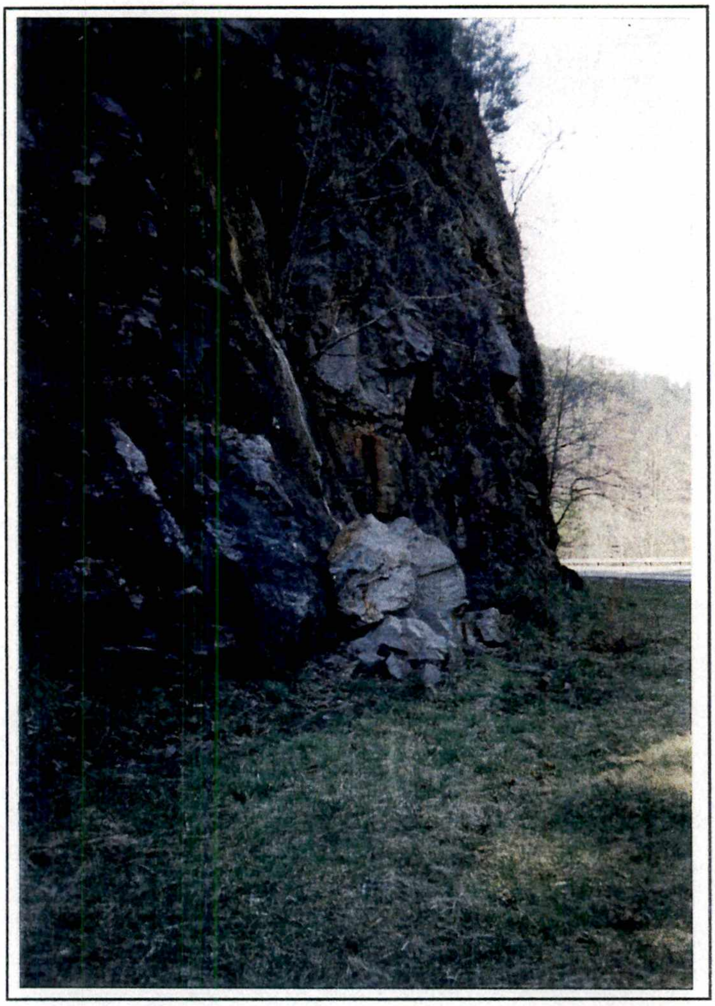

A-6.b Massive rock formations is the singular characteristic of the slope.

APPENDIX B

Views of The Beddings and Folds in Rock Cut 1

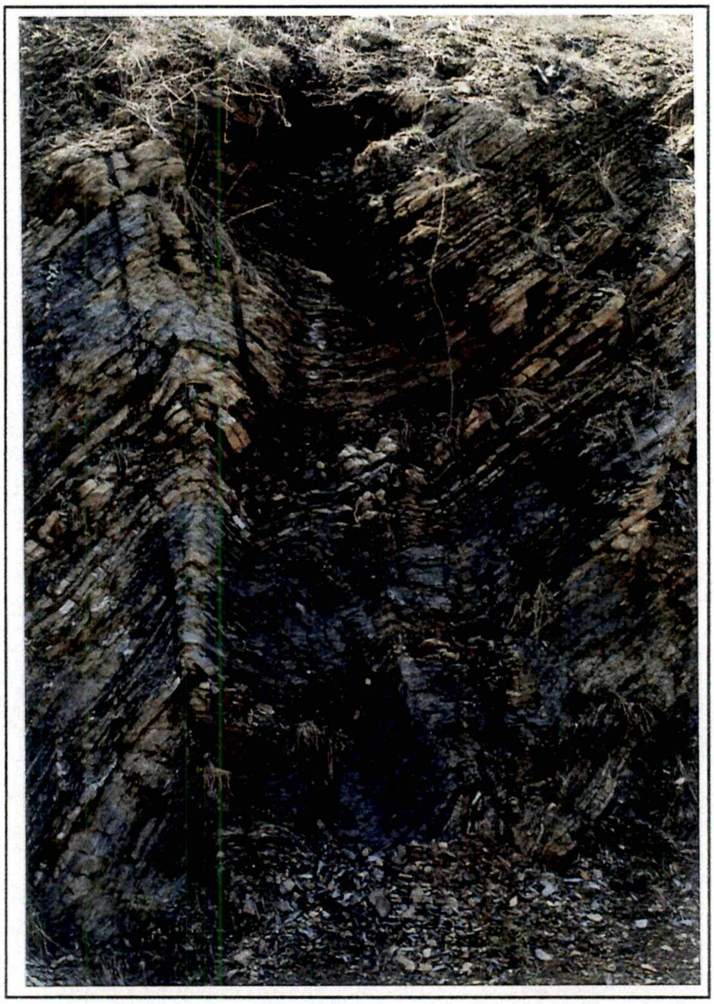

B-1.a Folded rock still showing the tracks of the boreholes on it.

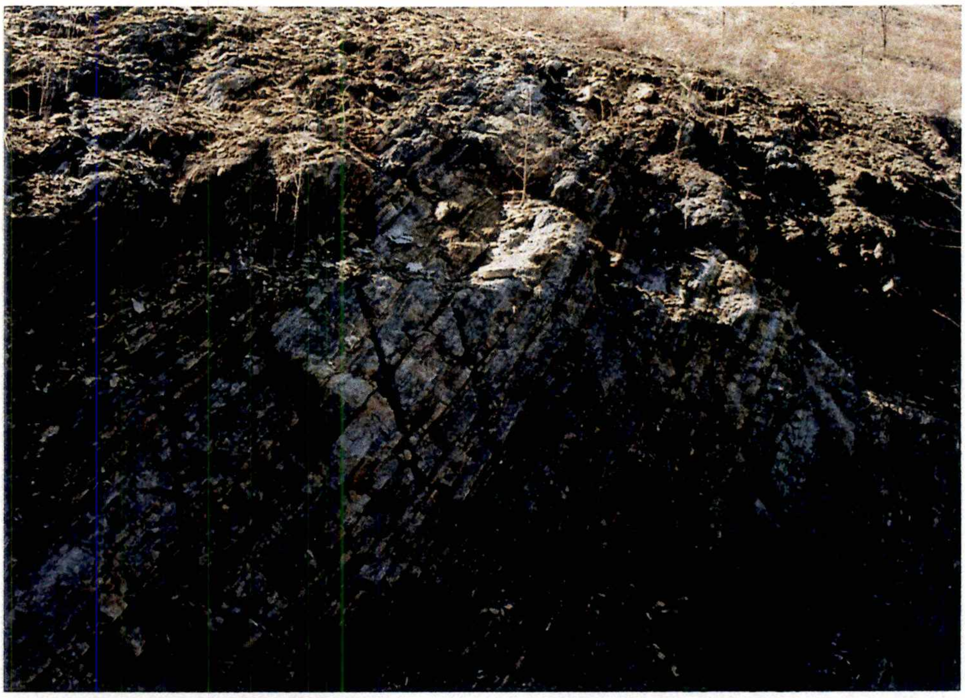

B-1.b Bedding planes dipping southeastward.

B-1.c One of the typical folded rocks in this section.

Three Different Aspects of the Rock Formations in Rock Cut 3

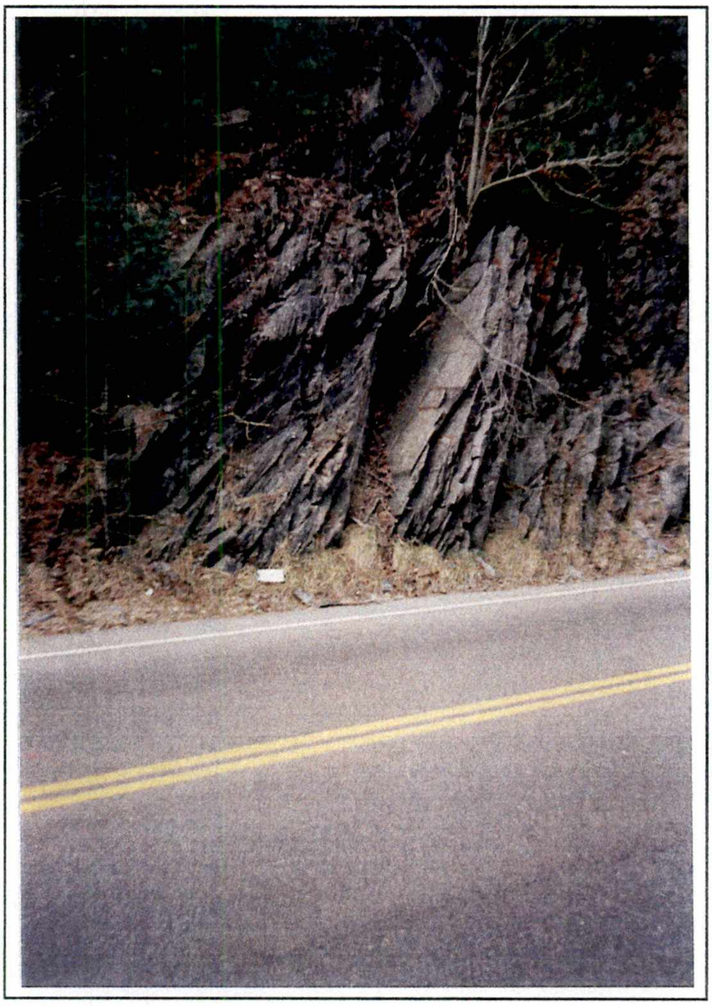

B-3.a Another view of the steeply inclined bedding.

B-3.b View of a thighly folded rock. Arrows indicate direction of the bedding planes.

B-3.c Open fold with presence of cleavage on it trending northeastward

APPENDIX C

Computer Program

```
1  REM***General solution for Prismatic Rock Blocks*******
5  REM****by Jorge A. Ureta and Matthew Mauldon*******
10 REM***This program has the finality of giving the normal forces
15 REM***acting on the discontinuity planes and the safety factor
20 REM***of prismatic blocks when sliding parallel to the line of
25 REM***intersection common to a set of failure planes.
30 CLS
40 cons = 3.141592654# / 180
50 DIM m(20), DIP(20), DD(20), theta(20), L(20), A(200), beta(200)
60 DIM NUM(200, 20), DEN(200, 20), N(200), D(200), R(200), S(200), s1(20)
70 DIM s2(20), F(20), T2(200), k(20), B(20), H(20), P1(20), Q2(20), R3(20)
80 DIM alpha(20), SUM(20), SUM1(20), SUMx(20), SUMy(20)
90 REM***Input data to be given from the screen***
100 OPEN "RESULT.dat" FOR OUTPUT AS #1    'to store results in an output file
110 INPUT "angle of resultant in XZ plane = ", T
120 INPUT "components of resultant force: (x,y,z) = ", FR(1), FR(2), FR(3)
130 INPUT "Do you want to enter fold axis directly: (y/n)?", mm$
140 IF mm$ = "y" THEN GOTO 900
150 IF mm$ = "n" THEN GOTO 170
160 REM***Calculation of the Safety Factor using dip and dip directions***
170 INPUT "Give the number of planes with Dip and DD = ", m
180 PRINT #1, "Plane #", "DIP", "DIP DIRECTION"
190 PRINT #1,
200 REM***Input numering of planes in order from north***
210 FOR I = 1 TO m     'increment of planes
220 INPUT "values of Dip and DD are =", DIP(I), DD(I)
230 PRINT #1, I, DIP(I), DD(I)
240 NEXT I
250 PRINT #1,
260 REM***Calculation of normal vectors of each plane***
270 PRINT #1, "Plane #", "l", "m", "n"    'components of the normal vectors
290 PRINT #1,
300 FOR I = 1 TO m
310 DIP(I) = DIP(I) * cons
320 DD(I) = DD(I) * cons
330 x(I) = SIN(DIP(I)) * SIN(DD(I))
340 y(I) = SIN(DIP(I)) * COS(DD(I))
350 z(I) = COS(DIP(I))
360 PRINT #1, I, x(I), y(I), z(I)
```

```
370 PRINT USING "##.#####  "; I; x(I); y(I); z(I)  'normal components on screen
380 NEXT I
390 REM***Direction of Resultant Force-X:east, Y:north, Z:up***
400 PRINT "Input numering of planes in order from north" 'stereographic method
410 PRINT #1,
420 PRINT
430 INPUT "Initial plane = ", I
440 IF I = 0 THEN GOTO 1390
450 P(I) = y(I) * z(I + 1) - y(I + 1) * z(I)
460 Q(I) = -(x(I) * z(I + 1) - x(I + 1) * z(I))
470 R(I) = x(I) * y(I + 1) - x(I + 1) * y(I)
480 C1 = SQR(P(I) ^ 2 + Q(I) ^ 2 + R(I) ^ 2)
490 IF C1 < 1E-08 THEN PRINT "C1 = 0"
500 P1(I) = P(I) / C1   'components of the intersection line
510 Q2(I) = Q(I) / C1
520 R3(I) = R(I) / C1
530 PRINT #1, "Vector of intersection between  "; I; "and "; I + 1
540 PRINT #1, "I = "; "("; P1(I); ")"; "i + "; "("; Q2(I); ")"; "j + "; "("; R3(I); ")";
550 PRINT #1, "k"
560 PRINT "Vector of intersection between  "; I; "and "; I + 1
570 PRINT "I = "; "("; P1(I); ")"; "i + "; "("; Q2(I); ")"; "j + "; "("; R3(I); ")"; "k"
580 REM***Dot Product between R and I***
590 DP(1) = FR(1) * P(I)
600 DP(2) = FR(2) * Q(I)
610 DP(3) = FR(3) * R(I)
620 DRP = DP(1) + DP(2) + DP(3)
630 PRINT #1, "DRP = "; DRP
640 PRINT "DRP = "; DRP
650 REM***Calculation of RN, RT, RNv, and RTv***
660 RT = ABS(DRP / C1)      'RT (driving force)
670 RTv(1) = DRP * P(I) / (C1) ^ 2      'components of RT
680 RTv(2) = DRP * Q(I) / (C1) ^ 2
690 RTv(3) = DRP * R(I) / (C1) ^ 2
700 RNv(1) = FR(1) - RTv(1)             'components of RN
710 RNv(2) = FR(2) - RTv(2)
720 RNv(3) = FR(3) - RTv(3)
730 RN = SQR(RNv(1) ^ 2 + RNv(2) ^ 2 + RNv(3) ^ 2)  'RN (resisting force)
740 REM***Results stored in output file***
750 PRINT #1, "RT = "; RT
760 PRINT #1, "RTv = "; "("; RTv(1); ")"; "i + "; "("; RTv(2); ")"; "j + "; "(";
770 PRINT #1, RTv(3); ")"; "k"
780 PRINT #1, "RN = "; RN
790 PRINT #1, "RNv = "; "("; RNv(1); ")"; "i + "; "("; RNv(2); ")"; "j + "; "(";
800 PRINT #1, RNv(3); ")"; "k"
```

```
810 REM***Results on the screen***
820 PRINT "RT = "; RT
830 PRINT "RTv = "; "("; RTv(1); ")"; "i + "; "("; RTv(2); ")"; "j + "; "("; RTv(3);
840 PRINT ")"; "k"
850 PRINT "RN = "; RN
860 PRINT "RNv = "; "("; RNv(1); ")"; "i + "; "("; RNv(2); ")"; "j + "; "(";
870 PRINT RNv(3); ")"; "k"
880 GOTO 410
890 REM***Calculation of the intersection line using pl. and tr. of the fold axis"***
900 PRINT
910 PRINT "(enter value of angles in degrees)"
920 INPUT "enter plunge and trend of intersection line: (pl,tr) = ", PL, TR
930 PRINT #1, "intersection line : "; "plunge = "; PL, "trend = "; TR
940 REM***Calculation of the components of the intersection line***
950 PRINT #1,
960 PL1 = PL * cons
970 TR1 = TR * cons
980 x1 = COS(PL1) * SIN(TR1)
990 y1 = COS(PL1) * COS(TR1)
1000 z1 = -SIN(PL1)
1010 PRINT "Vector of intersection I"
1020 PRINT "I = "; "("; x1; ")"; "i + "; "("; y1; ")"; "j + "; "("; z1; ")"; "k"
1030 PRINT #1, "Vector of intersection I"
1040 PRINT #1, "I = "; "("; x1; ")"; "i + "; "("; y1; ")"; "j + "; "("; z1; ")"; "k"
1050 REM***Dot Product between R and I***
1060 DP1 = FR(1) * x1
1070 DP2 = FR(2) * y1
1080 DP3 = FR(3) * z1
1090 DPR = DP1 + DP2 + DP3
1100 PRINT #1, "DPR = "; DPR
1110 PRINT "DPR = "; DPR
1120 REM***Calculation of RN, RT, RNv, and RTv***
1130 RT = ABS(DPR)   'value of RT (driving force)
1140 RTv1 = DPR * x1    'components of RT
1150 RTv2 = DPR * y1
1160 RTv3 = DPR * z1
1170 RNv1 = FR(1) - RTv1      'components of RN
1180 RNv2 = FR(2) - RTv2
1190 RNv3 = FR(3) - RTv3
1200 RN = SQR(RNv1 ^ 2 + RNv2 ^ 2 + RNv3 ^ 2)   'value of RN (resisting force)
1210 REM***Results stored in output file***
1220 PRINT #1, "RT = "; RT
1230 PRINT #1, "RTv = "; "("; RTv1; ")"; "i + "; "("; RTv2; ")"; "j + "; "("; RTv3;
1240 PRINT #1, ")"; "k"
```

```
1250 PRINT #1, "RN = "; RN
1260 PRINT #1, "RNv = "; "("; RNv1; ")"; "i + "; "("; RNv2; ")"; "j + "; "(";
1270 PRINT #1, RNv3; ")"; "k"
1280 REM***Results on the screen***
1290 PRINT "RT = "; RT
1300 PRINT "RTv = "; "("; RTv1; ")"; "i + "; "("; RTv2; ")"; "j + "; "("; RTv3;
1310 PRINT ")"; "k"
1320 PRINT "RN = "; RN
1330 PRINT "RNv = "; "("; RNv1; ")"; "i + "; "("; RNv2; ")"; "j + "; "("; RNv3;
1340 PRINT ")"; "k"
1350 INPUT "continue (y/n)? ", jor$
1360 IF jor$ = "y" THEN GOTO 1390
1370 IF jor$ = "n" THEN GOTO 2260
1380 REM***Solution of equation (18) for every value of A***
1390 PRINT
1400 PRINT #1,
1410 INPUT "Give number of planes measured clockwise from X axis = ", k
1420 PRINT #1, "Plane #", "angle from X", "length (cm)"
1430 PRINT #1,
1440 FOR I = 1 TO k
1450 INPUT "(angle of plane,length of plane) = ", theta(I), L(I)
1460 PRINT #1, I, theta(I), L(I)
1470 NEXT I
1480 PRINT #1,
1490 FOR A = 0 TO 180 STEP .5   'if intergers are used step 0.5 must be erased
1500 beta(A) = A * cons
1510 FOR I = 1 TO k
1520 alpha(I) = theta(I) * cons
1530 t1 = T * cons
1540 T2(A) = TAN(beta(A) - t1)
1550 REM***NUM(A,I) is the numerator and DEN(A,I) is the denominator of eq. 18
1560 NUM(A, I) = L(I) * SIN(beta(A) - alpha(I)) * COS(beta(A) - alpha(I))
1570 DEN(A, I) = L(I) * (COS(beta(A) - alpha(I))) ^ 2
1580 IF COS(beta(A) - alpha(I)) <= 0 THEN NUM(A, I) = 0: DEN(A, I) = 0
1590 NEXT I
1600 NEXT A
1610 REM***Calculation of s1 and s2 (displacements)***
1620 PRINT #1,
1630 PRINT #1, "s1", "s2", "Avg.", "%", "theta s"
1640 PRINT #1,
1650 FOR A = 0 TO 180 STEP .5   'if integers are used step .5 must be erased
1660 N(A) = 0      'use .0000001# if there is a message of division by zero
1670 D(A) = 0      'the same condition mentioned above
1680 FOR I = 1 TO k
```

```
1690 N(A) = N(A) + NUM(A, I)
1700 D(A) = D(A) + DEN(A, I)
1710 NEXT I
1720 R(A) = N(A) / D(A)
1730 S(A) = R(A) - T2(A)
1740 IF (S(A) > .5) OR (S(A) < -.5) THEN GOTO 1800
1750 s1 = (SIN(beta(A) - t1)) / N(A)    'displacement using eq. 12
1760 s2 = (COS(beta(A) - t1)) / D(A)    'displacement using eq. 13
1770 PRINT #1, s1, s2, (s1 + s2) / 2, 2 * 100 * (s1 - s2) / (s1 + s2), A
1780 PRINT USING "##.#####    "; s1; s2; (s1 + s2) / 2;
1790 PRINT 2 * 100 * (s1 - s2) / (s1 + s2); A
1800 NEXT A
1810 REM***Calculation of the normal forces acting on each plane***
1820 INPUT "Avg. = ", P  'use avg. between s1 and s2 or one of them
1830 INPUT "angle theta* = ", z   'value of A for which a minimum is reached
1840 INPUT "Friction Angle =", w  'friction angle assumed equal for all planes
1850 PRINT #1,
1860 PRINT #1, "plane", "Fn"
1870 PRINT #1,
1880 FOR I = 1 TO k
1890 z1 = z * cons
1900 F(I) = L(I) * P * COS(z1 - alpha(I)) * RN  'Rn according to line 545 or 960
1910 IF COS(z1 - alpha(I)) <= 0 THEN F(I) = 0
1920 PRINT #1, I, F(I)
1930 PRINT I, F(I)
1940 B(I) = F(I)
1950 NEXT I
1960 phi = w * cons
1970 H = 0
1980 FOR I = 1 TO k
1990 B(I) = H + B(I)
2000 H = B(I)
2010 NEXT I
2020 SF = H * TAN(phi) / RT
2030 PRINT #1, "friciton angle = "; w, "SF = "; SF
2040 PRINT "SF = ", SF
2050 REM***Calculation of equilibrium in plane XY***
2060 PRINT #1,
2070 PRINT #1, "Equilibrium of forces"
2080 PRINT #1,
2090 SUMx = 0
2100 SUMy = 0
2110 FOR I = 1 TO k
2120 SUM(I) = SUMx + F(I) * COS(alpha(I)) * (-1)
```

```
2130 SUM1(I) = SUMy + F(I) * SIN(alpha(I))
2140 SUMx = SUM(I)
2150 SUMy = SUM1(I)
2160 NEXT I
2170 PRINT #1, "Equilibrium on X direction -->", SUMx + (RN * COS(t1))
2180 PRINT #1, "Equilibrium on Y direction -->", SUMy - (RN * SIN(t1))
2190 PRINT "SUMx = ", SUMx + (RN * COS(t1))
2200 PRINT "SUMy = ", SUMy - (RN * SIN(t1))
2230 INPUT "Continue (y/n)= ?", ans$
2240 IF ans$ = "y" THEN GOTO 1840
2250 IF ans$ = "n" THEN GOTO 2260
2260 CLS
2270 CLOSE #1
2280 END
```

VITA

Jorge Antonio Ureta Reyes was born in David, Panamá on October 14, 1959. He attended La República de Francia elementary school and graduated from Félix Olivares Contreras secondary school in 1977.

He entered La Universidad Tecnológica de Panamá in David in April 1978, and received the Bachelor of Science degree in Civil Engineering in 1985.

From April 1986 to December 1991, Mr. Ureta worked in La Universidad Tecnológica de Panamá at David as an Assistant Professor. From April 1986 to March 1990, Mr. Ureta was in charge of the Concrete and Soil Mechanics Laboratory and teaching at the same time courses such as Soil Mechanics, Structure I, Vector Analysis, and Survey I to Civil Engineering students; other courses taught by Mr. Ureta are Basic Static, Soil Mechanics, and Concrete Design to Technicians in Construction. From March 1990 to December 1991, Mr. Ureta was just dedicated to teach to engineering students. In November 1991, he was elected for a scholarship granted by LASPAU-Fulbright to do Master studies in the United States at the University of Tennessee - Knoxville. The studies began on August 26, 1992, and finished on August 12, 1994.

Mr. Ureta is married to the former Ana Elida Acosta of David, Panamá, and has two daughters, Carol Ariadne and Milena Dessireé.